p-Type Cu_2O/PEI modified Si-Nanowires for Efficient Liquid Junction Solar Cells

A Project Report Submitted

as part of the requirements for the degree of

MASTER OF SCIENCE

By

SAURABH KUMAR PATHAK

Roll No. CY19MSCST11027

Under the supervision of

Prof. M. DEEPA

to the

DEPARTMENT OF CHEMISTRY

INDIAN INSTITUTE OF TECHNOLOGY HYDERABAD

INDIA

APRIL, 2021

APPROVAL SHEET

This thesis entitled "**p-Type Cu_2O/PEI modified Si-Nanowires for Efficient Liquid Junction Solar Cells**" by **Saurabh Kumar Pathak** is approved for the degree of Master of Science from IIT Hyderabad.

Prof. Ch. Subrahmanyam

Professor

Department of Chemistry

Examiner

Dr. Surendra Kumar Martha

Associate Professor

Department of Chemistry

Examiner

Dr. Praveen Meduri

Associate Professor

Department of Chemical Engineering

Examiner

Prof. M Deepa

Professor

Department of Chemistry

Advisor

Declaration

I hereby declare that the matter embodied in this report is the result of investigation carried out by me in the Department of Chemistry, Indian Institute of Technology Hyderabad, under the supervision of Prof. M. Deepa.

In keeping with general practice of reporting scientific observations, due acknowledgement has been made wherever the work described is based on the findings of other investigators.

Signature of the Supervisor

(Signature)

SAURABH KUMAR PATHAK

(Student Name)

CY19MSCST11027

(Roll Number)

Acknowledgments

I would like to express my sincere gratitude to my supervisor **Prof. M. Deepa** for her constant support and motivation throughout my project. I feel grateful to have been allowed to work under her superb guidance. Her continuous support and encouragement have helped me work honestly towards my goal. Her knowledge, understanding, and expertise have helped me immensely in the completion of my research work and the organization of my thesis.

I would also like to thank **Ms. Ankita Kolay** and **Mr. Debanjan Maity** for their constant support and motivation. Their strong understanding of the concepts and ability to explain them with ease has helped me understanding things in a better way. Their positive guidance during this challenging time has enabled me to work with a positive mindset. I would also like to thank my seniors Mr. Manoranjan Ojha, Mr. Sathish Deshagani, Ms. Ishita Naskar, and Mr. Souvik Naskar, and my friends Karisma, Abhay, Aanshi, Uddeshya, and Prachi for their encouragement and cooperation during the research project.

I am grateful to the head of the department of chemistry, Prof. G. Satyanarayana, and to the entire Department of Chemistry, IIT Hyderabad, for allowing me to do research.

Finally, I would like to thank my parents and my brother, who always boost my morale, and without them, this work could have been impossible.

Abstract

This work aims at fabricating an efficient liquid junction silicon nanowire solar cell and investigate their photovoltaic performance. Here, p-type Cu_2O is used as a hole conductive material and is synthesized using the hydrothermal method. The silicon nanowires are etched on an n-Si wafer using metal-assisted chemical etching, and to avoid agglomeration, they are treated with 5% HF. The carbon fabric is used as a counter electrode due to its stability and high conductivity instead of previously reported Pt metal as a counter electrode which was very expensive. 0.05 M HBr and 8.6 M Br_2 mixture is used as a redox solution. In the case of SiNW, the efficiency obtained was 5.04% which is attributed to the light trapping properties of SiNW, and also in the case of Cu_2O microcrystals decorated SiNW, the efficiency obtained was 5.08% which is almost the same as in the case of SiNW this can be explained by the fact that the HOMO of Cu_2O is not aligned properly to act as hole conductor but as soon as the Cu_2O@SiNW is further coated with PEI polymer the efficiency increases by about 50% which can be explained by the fact that as the Cu_2O microcrystals are decorated with PEI polymer, it decreases its work function and due to which its HOMO come above the HOMO of the SiNW and it acts as hole conducting material. In previous reports, metal nanoparticles, i.e., Pt and Au, are used over SiNW act as electron trappers, but PEI decorated SiNW act as hole conductor, due to which the recombination rate decreases and overall performance of the cell increases. The hole conducting property of PEI@Cu_2O can be proved by the fact that in the case of Cu_2O@SiNW, the efficiency is 5.08%, same as in the case of pristine SiNW, but in the case of PEI@Cu_2O@SiNW, the efficiency is 7.65%, about 1.5 times increase in efficiency is observed. Various characterization including optical, structural, impedance studies, PEC are performed to understands the phenomenon deeply, which is involved in improved performance of PEI@Cu_2O@SiNW photoanode.

Contents

List of figures

List of tables

List of Figures

List of Tables

1. INTRODUCTION

In today's world, the major problem that humanity is facing is the global energy problem, and the main reasons behind this are increased global energy demand with the rise in population, depletion of fossil fuels, and pollution caused by the non-renewable source of energies. Humans consume approximately 17.4 TW in a year (2015), and it is estimated that energy demand will increase by 53% from 2010 to 2035. [1] So, to tackle the global energy problems and to replace non-renewable energy, we need an alternative energy source that is clean and safe for the environment and also fulfills the global energy demand. The best alternative source of energy is our sun which provides the earth with 174 000 TW power in a year or, in other words, the amount of energy that hits the earth in 1 hrs. is more as compared to the energy used by our planet in an entire year. [39] Hence, we need a device that can convert solar energy into electricity. A solar cell is a device that converts light energy directly into electrical energy by the photovoltaic effect. The first solar cell was demonstrated in 1954 by Chapin et al. at Bell Lab, which showed 6% efficiency. [2] The first generation of solar cells includes polycrystalline and monocrystalline silicon as semiconductors and can achieve power conversion efficiency up to 25% [3] and dominates the market, but the major drawback is high cost and complex fabrication. Therefore, low cost and easy to fabricate alternatives are needed. The second-generation solar cells include materials such as Si thin films, mc-Si cells, CdTe cells (PCE ≈ 20%), CIS, and CIGS cells (PCE ≈ 20%) [3]. The advantage of these cells is the high absorption coefficient and low cost, but again we have the disadvantages like environmental contamination, and the materials used to make the solar cell are hard to find. The third-generation solar cell includes materials such as Nanocrystal, polymer, dye-sensitized solar cells (PCE ≈ 13%), [4, 5] organic solar cells (PCE ≈ 11%), [3] quantum dots solar cells (PCE ≈ 6−10%), [6] perovskite solar cells (PCE ≈19.3%) [7], etc. The advantage of these solar cells is that they require a low cost to produce, easy to fabricate, and raw materials are easy to find, but the disadvantage is their low efficiency compared to commercial solar cells; hence extensive research and development is going on to make them more efficient. A very recent area of research and development in solar cells is Silicon Nanowire-based solar cells. In 1964, Wagner and Ellis first reported the synthesis of silicon nanowire (SiNW) using vapor-liquid-solid (VLS) growth using

gaseous silane (SiH_4) as precursor and gold (Au) nanoparticles as catalysts [8]. In the last 20 years, SiNW have gained a lot of attention due to their application in electronic devices such as solar cells, field-effect transistors(FET), and also as biological sensors. There are various methods available for etching of SiNW, such as laser beam ablation, [9] ion beam etching, [10] thermal evaporation oxide-assisted growth [11], but nowadays, the most efficient method to etch SiNW is MaCE (Metal-assisted chemical etching) [12]. SiNW gained a lot of attention worldwide because of their unique properties such as earth abundance, non-toxicity, and their 1D structure allows efficient electron transport due to quantum confinement and has better optical and electrical properties compared to planar silicon. Bare SiNW are very much unstable and prone to oxidation, so it is terminated using H and alkyl group to provide stability also they are decorated with either metal or semiconductor nanoparticles to improve exciton transport.[14, 17] The redox electrolyte used in SiNW solar cell provides better ionic conductivity between the electrodes, which helps in quick transportation of holes which oxidizes the reduced species of the electrolyte and reduces the oxidized species of the electrolyte by capturing an electron from the counter electrode. The counter electrode material catalyzes the regeneration of redox electrolyte by reduction. The disadvantages of liquid junction solar cells are that the aqueous electrolyte used is corrosive and can deteriorate cell efficiency, so a non-aqueous electrolyte is used to avoid it. To improve the stability of the liquid junction silicon nanowire devices, the highly volatile and flammable organic solvents like acetonitrile and methanol are replaced with solvent-free Ionic Liquid (IL) electrolyte. Although SiNW based solar cells have lower efficiency as compared to conventional solid-state solar cells, there are a lot of possibilities for the modification in the structure, electrolyte, and electrode used in the cell to get a more efficient and stable solar cell.

1.1 Basics of Solar Cell

1.1.1 Semiconductor

- These are the elements in the periodic table whose conductivity lies between that of non-metals and most of the metals having range 10^{-6}-10^{4} ohm^{-1} cm^{-1}.
- They are of two types:
    - **p-type** semiconductors in which conduction occurs due to holes.
    - **n-type** semiconductors in which conduction occurs due to electrons.
- They have a wide range of applications because their conductivity can be changed by adding a small amount of impurity and are widely used to make IC and solar cells.

1.1.2 Structure of Semiconductor

- The semiconductor can be from group IV of the periodic table of the semiconductor can be combined into two groups, i.e., III-V (GaAs) or II-VI (ZnS).
- The most widely used semiconductor is silicon and has got four valence electrons which are involved in the formation of four covalent bonds with four surrounding silicon atoms.
- Semiconductors usually don't conduct electricity at room temperature, but as the temperature is increased, the electrons forming covalent bonds get excited from valence band (HOMO) to conduction band (LUMO) and participates in conduction.

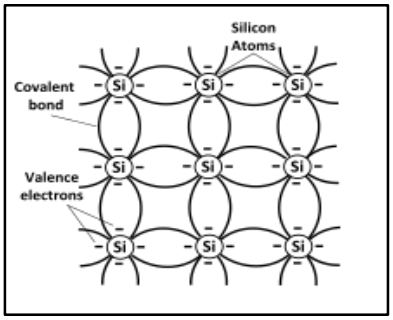

Fig 1.1.2: Covalent bonding in silicon (nb: Si bonds are not in a square grid)

1.1.3 Solar Cell

- It is a device that is used to convert optical energy into electrical energy.
- The solar cell works in the wide spectral range, which is known as the solar spectrum.
- Three relevant bands in the solar spectrum are UV, visible and infrared.
- The light that is reaching to earth's surface consists of 49.4% infrared, 42.3% visible, and 8% of UV radiation. [18]
- In the atmosphere, the path length of light depends on its angle of incidence, and it keeps changing throughout the day and is defined by using **AIR-MASS NUMBER (AM).**

1.1.4 Air-Mass Number (AM): It is defined as the secant of the angle between the sun and the zenith.

- **AM0:** It is the solar spectrum outside the earth's atmosphere.
- **AM1:** When the angle is 0^{o}, i.e., the sun is at the zenith, it has the intensity of 0.925 KWm^{-2}.
- **AM1.5:** Angle is 48.2^{o}, and 1 sun is equal to 1 KWm^{-2} of irradiance.
- **AM2:** when the angle is 60^{o} and intensity is 0.691 KWm^{-2}

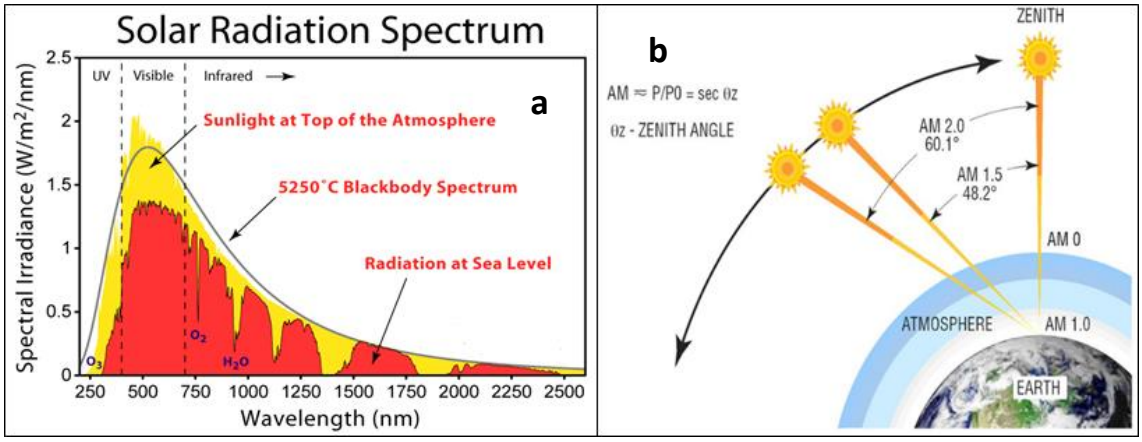

Fig 1.1.4: a) Solar Radiation Spectrum; b) Air mass number at different zenith angle

1.2 Solar Cell Parameters

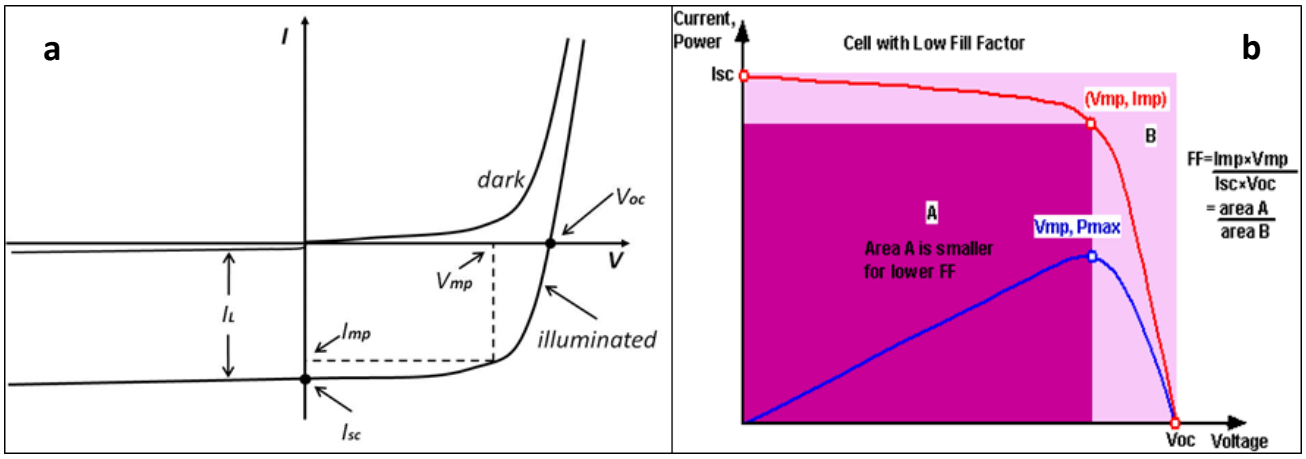

Fig 1.2: a) The Graph of the I-V characteristics of an ideal diode solar cell when non-illuminated (dark) and illuminated; b) Graph depicting various solar cell parameters

1.2.1 IV characteristic:

- It is defined as the superposition of the IV curve of solar cell diode obtained in the dark with that of light-generated current.
- In the dark, the IV curve has the same characteristic as that of a simple diode.
- When light shines, the curve shifts as the cell starts generating power.
- The amount of shift depends on the intensity of light and is directly proportional to intensity.
- By convention, the obtained curve is flipped.

1.2.2 Short-Circuit Current (I_{sc})

- The short circuit current is the current obtained when voltage is zero across the solar cell or the maximum current that can be obtained from the solar cell.
- The short circuit current depends on various factors like the cell area, light intensity, the spectrum of light incident on the cell, the absorption and reflectance property of the cell, and the carrier collection property.
- Short circuit current decreases with an increase in the bandgap.

1.2.3 Open-Circuit Voltage (V_{oc})

- It is defined as the voltage obtained when the current is zero across the solar cell.
- V_{oc} depends on saturation current and light generated current of the solar cell.

- Open-circuit voltage increases with an increase in the bandgap.

1.2.4 Fill-Factor (FF)

- The fill factor is the ratio of maximum power obtained from the solar cell (P_{mp}) to that of the product of V_{oc} and I_{sc}. **[FF = $P_{mp}/V_{oc}*I_{sc}$].**

1.2.5 Power Conversion Efficiency (PCE)

- PCE is defined as the fraction of incident solar energy that gets converted to electrical energy.

1.3 Resistive Effects in Solar Cell

1.3.1 Characteristic Resistance

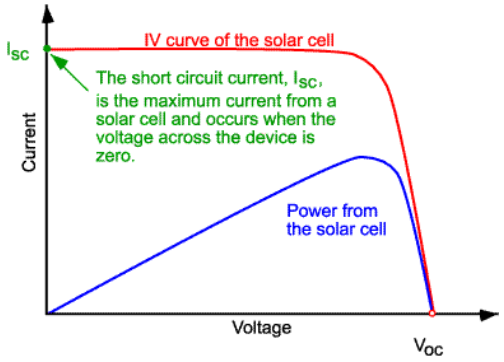

Fig 1.3.1 IV curve of a solar cell showing the open-circuit voltage.

- The cell's output resistance at its maximum power point is called its characteristic resistance. If the load resistance of the cell is equal to the cell's characteristic resistance, then the power transferred to the load is maximum. Mathematically, for most of the cells, it is defined as the ratio of V_{oc} to that of J_{sc}.

1.3.2 Effect of Parasitic Resistances

- Series resistance and shunt resistance are two of the most common parasitic resistance, and the figure below shows the inclusion of both the resistances in solar cell circuit. The general impact of parasitic resistance is that it decreases the fill factor.

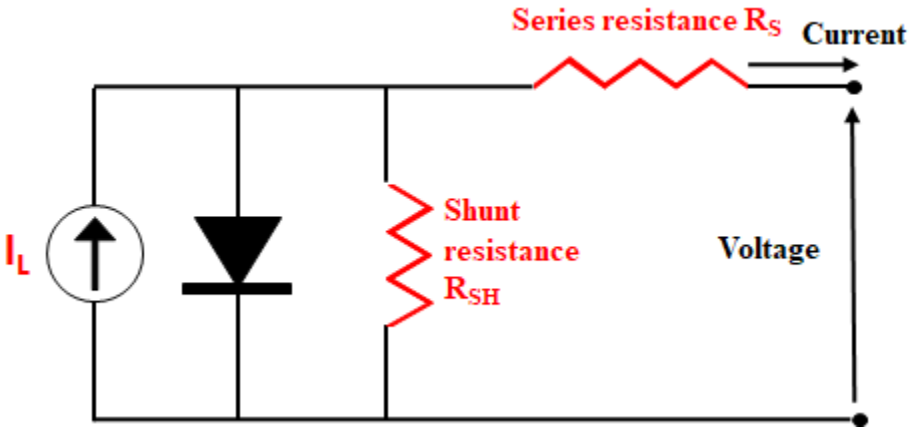

Fig 1.3.2: Parasitic series and shunt resistances in a solar cell circuit

1.3.3 Series Resistance

- Three primary sources due to which the series resistances arise are first, current flow through the emitter and base of the solar cell; second, the contact resistance at the interface of Metal and semiconductor; third, the metal contact at top and rear of the cell. Series resistance does not affect the cell at open-circuit voltage because the current flowing through the circuit is zero.

1.3.4 Shunt Resistance

- The primary source for the rise of shunt resistance is manufacturing defects. From the above circuit, we can conclude that if the shunt resistance is low, it will provide an alternate path for the current to flow, and hence it reduces the current flowing through the solar cell junction and reduces the voltage. The higher value of shunt resistance increases the output of the solar cell.

1.4 Generations of Solar Cells [19]

1.4.1 First Generation

Generally, 1st generation solar cells are silicon-based and have high efficiency in the 15-20% range; the maximum efficiency obtained is 25%. [20] They are four types based on the type of silicon used, i.e., monocrystalline silicon cells, polycrystalline silicon cells, amorphous silicon cells, hybrid silicon cells.

Advantages:

- High efficiency, Long lifetime

Disadvantages:

- Expensive, complex fabrication

1.4.2 Second Generation

To overcome the disadvantages of 1st generation solar cells, 2nd generation solar cells came into the picture. [21,22] They are generally based on thin-film solar cells and Si thin films, mc-Si cells, CdTe CIS, and CIGS cells. These cells have efficiency in the range of 10-15%.

Advantages:

- The high absorption coefficient, low cost

Disadvantages:

- Environment contamination, materials are hard to find

1.4.3 Third Generation

The high cost of 1st generation solar cells and toxicity and environmental concern caused by the 2nd generation solar cells led to the emergence of 3rd generation solar cells. [23] This generation used different materials besides silicon to fabricate solar cells, such as nanomaterials, silicon wires, solar inks.

Advantages:

- Raw materials easy to find, easy fabrication, minimal cost

Disadvantages:

- Liquid electrolyte, High-cost electrode, e.g., Pt, Ru

1.5 p-n junction

The p-type substrate has holes as majority charge carriers, whereas the n-type semiconductor has electrons as majority charge carriers. When p and n-type substrates are joined together, some holes from p-type substrates diffuse toward n-type, and some electrons from n-type diffuse toward p-type. This diffusion continues until the no of electrons and holes becomes the same on both sides. Due to diffusion at the p-n junction, there is the formation of the depletion region, which contains immovable charges which create potential difference across the junction.

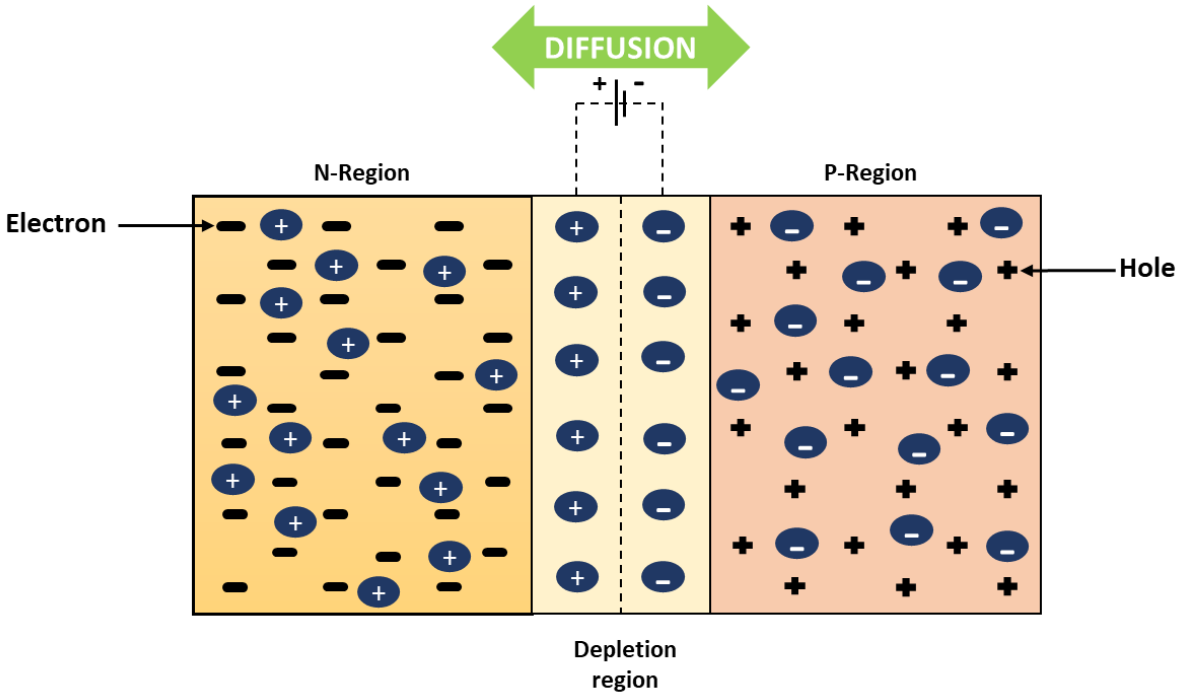

Fig 1.5: p-n Junction

1.6 Basic Working of Solar Cells

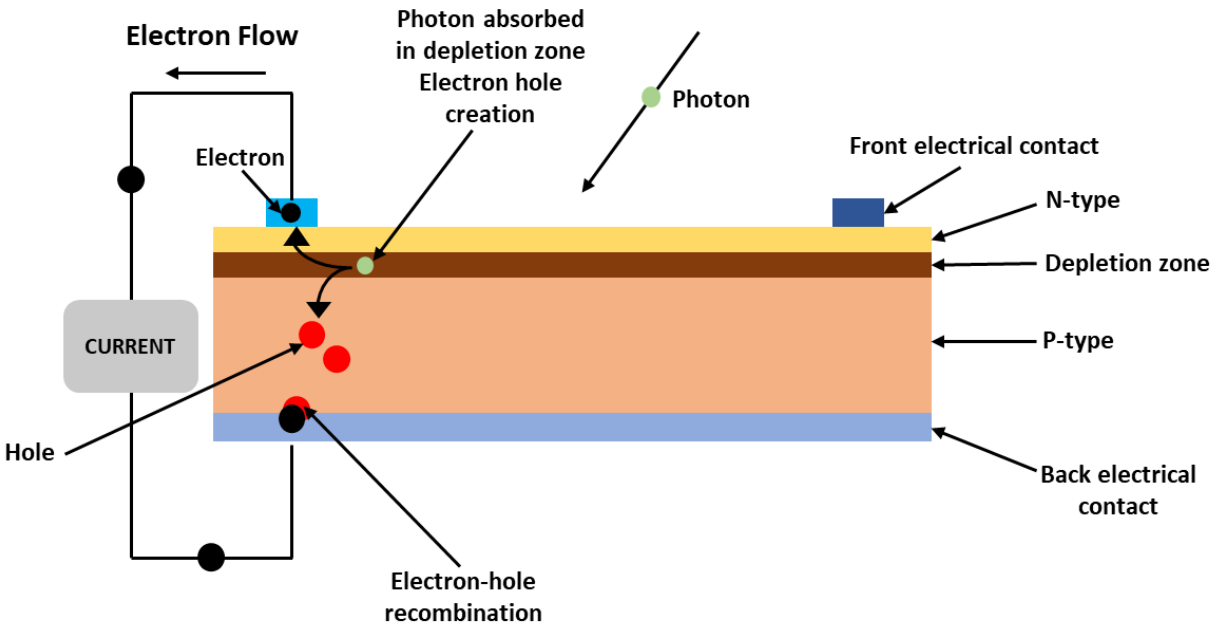

Fig 1.6: Basic working of Solar Cell

When p-type and n-type substrates are joined together, a region of immovable charge carriers is formed at the junction, which we call DEPLETION REGION. When a photon strikes the depletion region, it transfers enough energy to produce electron-hole pairs, due to which the thermal equilibrium at the junction gets disturbed. The electron in depletion travels to the n-side of the junction, whereas holes travel to the p-side. Once the electron travels to the n-side, it cannot cross the barrier potential at the junction, and also, holes cannot cross the potential barriers once they go to the p-type side. So from above, we can say that on the n-type side, we have an excess of electrons and excess holes on the p-type side, due to which a potential difference is set up across the p-n junction, and it behaves like a small battery cell. The voltage that we get across the junction is called photovoltage, and if we connect a load across the junction, we get a tiny current flowing through it.

1.7 The Shockley-Queisser Limit [24]

The Shockley-Queisser limit is the calculation of the maximum theoretical efficiency of a single PN junction solar cell. The maximum solar conversion efficiency calculated is around 33.7% assuming a single PN junction with a bandgap of 1.4 eV (using an AM 1.5 solar radiation), i.e., an ideal solar cell will generate 337 Wm^{-2} with incident solar radiation. When the solar radiation is approximated as 6000 K blackbody radiation, the maximum efficiency occurs when the bandgap is 1.4 eV.

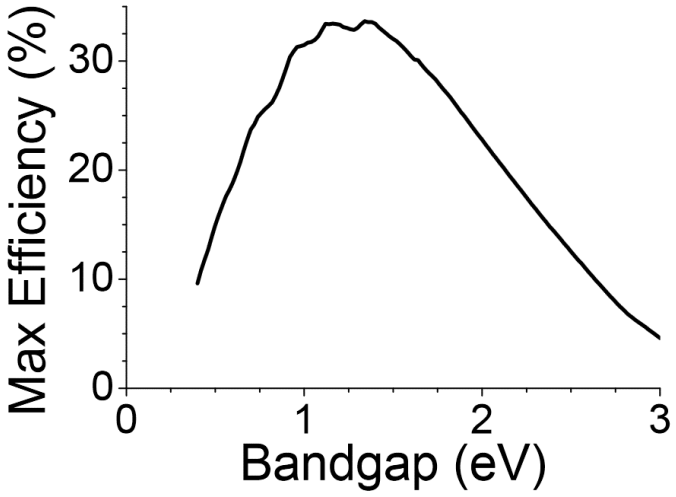

Fig 1.7: The Shockley–Queisser limit for the efficiency of a solar cell, without concentration of solar radiation.

Three primary things that are considered in the calculation are:

1.7.1 Blackbody radiation:

Whenever there is any type of energy loss within the cell ultimately turns into heat, so any inefficiency in the cell increases the cell temperature. The temperature keeps increasing until equilibrium is attained and is normally achieved around 360 K; hence the solar cell gives lower efficiency than their room temperature efficiency.

1.7.2 Recombination:

Recombination sets up an upper limit on the rate of electron-hole pair generation. So, due to recombination, there is about a 10% reduction in theoretical performance other than thermal losses. Open circuit voltage (V_{oc}) is limited by recombination.

1.7.3 **Spectrum losses:**

It is assumed that each absorbed solar photon gets converted into an electron flowing through the circuit. When the bandgap is high, then there are very few photons that have energy higher than the bandgap; hence the current density decreases, e.g., in the case of 1000 W/m^2 in AM1.5 solar radiations, 19% of photons have energy less than the bandgap of silicon, i.e., 1.1 eV and will not produce power in silicon cell.

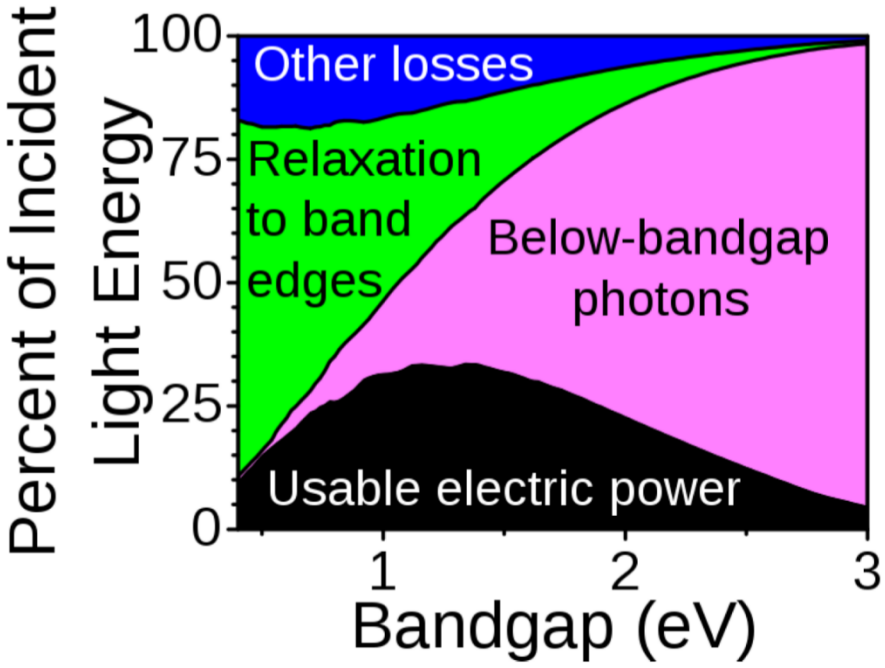

Fig 1.7.3: Breakdown of the causes for the Shockley–Queisser limit

1.8 **Silicon Nanowire (SiNW)** [25]

1.8.1 Properties of SiNW: Silicon nanowire (SiNW) are the type of nanowire made from silicon semiconductors as a precursor by etching on a solid silicon substrate or by catalyzed growth from vapor or liquid phase. There are various properties of SiNW that makes them a stronger candidate to be used in various application in future.

1.8.1.1 Mechanical Properties: Change in external factors such as temperature, external stress, and internal strain leads to internal dislocations, which ultimately change the conductivity of nanowire and hence are of great use in device processing. The high aspect ratio of SiNW than the bulk material reduces the number of defects present per unit length.

1.8.1.2 Electrical Properties: Nanowires have a large surface-to-volume ratio due to which their conductivity becomes very sensitive to surface excitation by external charges; hence a small change on the surface can influence the properties of the nanowire, this property of nanowires found to be useful in biosensor application. The 1D morphology of nanowires allows the electron to travel in only the axial direction and hole in the radial direction, which reduces the recombination rate hence is useful in solar cell application.

1.8.1.3 Chemical Properties: When the Si surface is exposed to air, it gets naturally oxidized. This phenomenon is useful in transistor and sensor applications. The oxidation on the surface can produce defects on the surface, which can act as a recombination site, and if there is a proper modification of the surface, the hole mobility can be increased.

1.8.1.4 Optical Properties: Polished Si wafer surface appears to be very shiny, but once the surface is etched to obtain SiNW, the surface becomes pitch black which occurs because of the light trapping properties of nanowires, and this property allows them to be used in solar cell application.

1.8.2 SiNW Synthesis

There are several methods available to synthesize SiNW and can be broadly divided into two methods based on the fact whether nanowires are obtained from bulk silicon or by using chemical or vapor precursor:

1.8.2.1 Top-Down Method (from bulk Si):

- Thermal evaporation oxide assisted [29]
- Laser beam ablation [26]
- Metal assisted chemical etching [28]
- Ion-beam etching [27]

1.8.2.2 Bottom-Up Method (using chemical or vapor precursor):

- Vapour liquid-solid method [26]

- Precipitation from solution [29]
- Molecular beam epitaxy [29]

So we have several methods to grow SiNW, but Metal assisted Chemical Etching (MaCE) is the most efficient technique available today to etch SiNW due to its properties such as low cost, high efficiency, no need for doping, obtained nanowires are robust, and do not peel off, and the SiNW etched are rough and non-reflective. The metal-assisted chemical etching technique is discussed in brief below.

1.8.3 Silicon Nanowire Solar Cells [30]

Solar cells in which the Silicon nanowires are used as photoanode are called Silicon nanowire solar cells. There are many properties of silicon nanowires that make them suitable for application in a solar cell:

- They are almost non-reflective due to their light scattering and absorption phenomenon.
- Since SiNW is directly obtained from bulk silicon, so there is no need for further doping.
- SiNW are an integral part of the substrate; hence they don't peel off from the substrate.
- 1D morphology of SiNW helps in radial junction charge transport.
- They have high electrical conductivity than bulk Si due to surface defects.
- They show an antireflective property in a wide range of spectral bandwidth, i.e., 300-1000 nm.
- SiNW based solar cells have low fabrication costs.

1.8.4 Liquid Junction Silicon Nanowire Solar Cells [31]

In liquid junction Silicon nanowire solar cells, the working electrode (SiNW) and the counter electrode are separated from each other with the help of liquid redox electrolyte between them. There are several advantages of liquid junction solar cells:

- In the case of the solid-state device, there is a need for processing for the formation of the diffused junction, but it is replaced by just putting the semiconductor in a liquid electrolyte.
- Electrolyte present in between cathode and anode helps to regenerate photoactive component of the electrode.

- Liquid electrolyte facilitates interfacial charge transfer and helps to maintain ionic conduction between electrodes.

1.8.5 Basic Device Architecture of Liquid Junction Silicon Nanowire Solar Cells

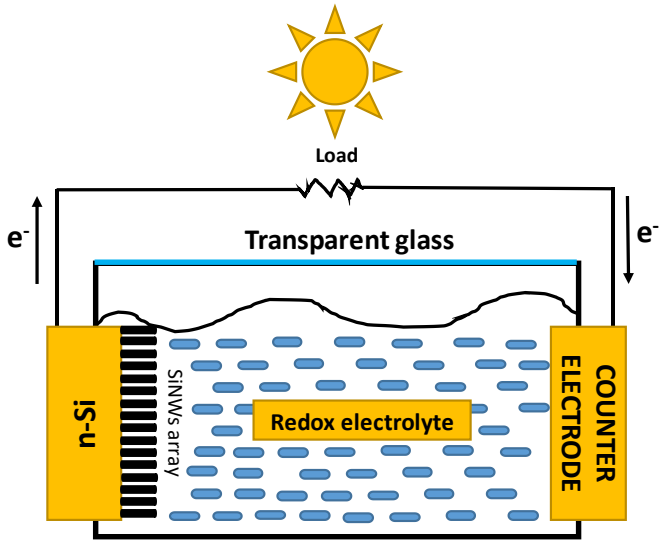

Fig 1.8.5: Basic structure of liquid junction solar cell

When light falls on SiNW through the transparent glass, then Photoexcited electrons are injected from SiNW to an external circuit, and holes are scavenged by electrolyte at electrode/electrolyte interface, and the redox electrolyte undergoes oxidation, the electron flows through an external circuit and get collected at counter electrode where it reduces redox electrolyte at counter electrode/electrolyte interface.

1.9 Literature Survey

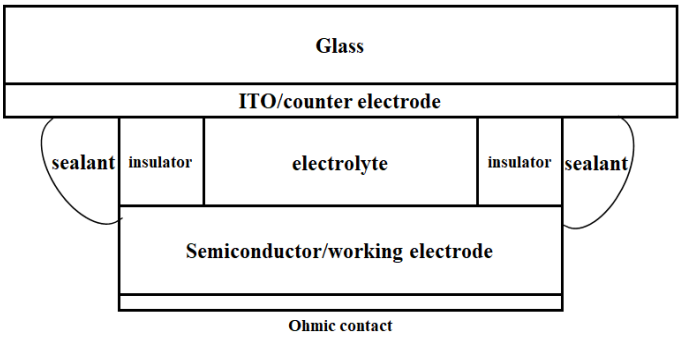

Figure 1.9.1. Cross-section of a typical thin-layer liquid junction solar cell

In 1984 Gibbsons et al. developed a planar silicon-based working electrode and ITO as a counter electrode in which non-aqueous solvent is used to avoid the photo corrosion of the electrode, and they also used an insulator between the working electrode and counter electrode to maintain interelectrode spacing and electrolyte used was "0.15-0.2 M 1, 1'-dimethylferrocene/0.15-0.2 M 1, 1'-dimethylferricenium tetrafluoroborate/1.0 M lithium perchlorate/methanol". In this solar cell parameters obtained are **V_{oc} = 0.60-0.61 V, J_{sc} = 28-34 mA/cm^2, FF = 0.69-0.77, PCE = 14.0 ± 1.0%. [13]**

In 1998 Bansal el al. terminated SiNW using alkyl chains and found that due to formation of Si-C covalent bond the SiNW are found to be much more stable and has better J-V characteristic as compared to H-terminated SiNW. They also tried to terminate the SiNW with higher alkyl chains and found that with the increase in alkyl chains, the performance of the cell deteriorated because of an increase in charge transfer resistance through thick alkyl over layer and $–CH_3$ terminated SiNW have the highest fill factor and stability as shown in table 1 below. The redox electrolyte used was $[Fe(CN)_6]^{3-/4-}$ and the counter electrode was Pt. **[14]**

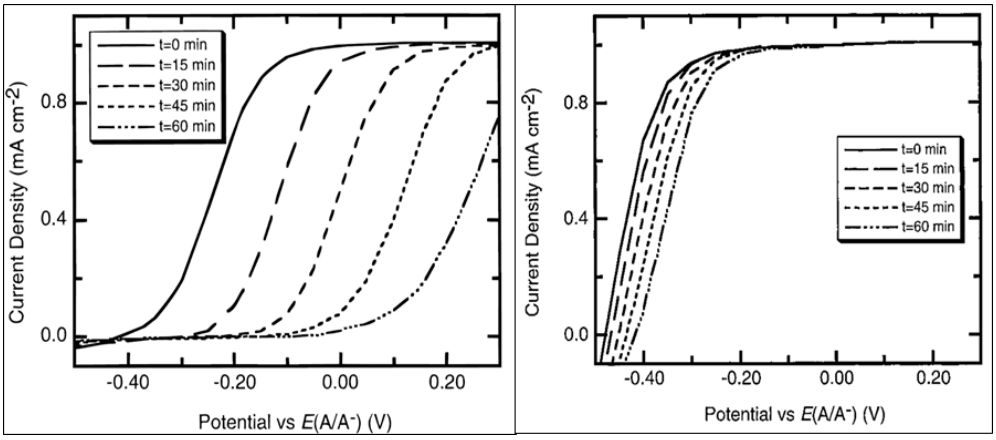

Fig 1.9.2. Time-dependence of the H-terminated and CH_3-terminated J-E behavior

TABLE 1: Current Density-Potential (J-E) Properties of H-Terminated and Alkyl-Terminated Si (111) Surfaces in Contact with 0.35 M $Fe(CN)_6^{4-}$-0.05 M $Fe(CN)_6^{3-}$(aq)

Terminal group	V_{oc}(V) t = 0 min	Fill factor t = 0 min	V_{oc}(V) t = 60 min	Fill factor t = 60 min
-H	0.42	0.34	0.22	0.08
$-CH_3$	0.48	0.64	0.42	0.57
$-C_2H_5$	0.45	0.53	O.35	0.46
$-C_4H_9$	0.40	0.22		
$-C_6H_{13}$	0.36	0.13		

In 2008 Peng et al. tried to etch the SiNW using two solutions that are HF-$AgNO_3$ and Ag-HF-H_2O_2, and found that SiNW etched using H_2O_2 were found to be much more regular. The

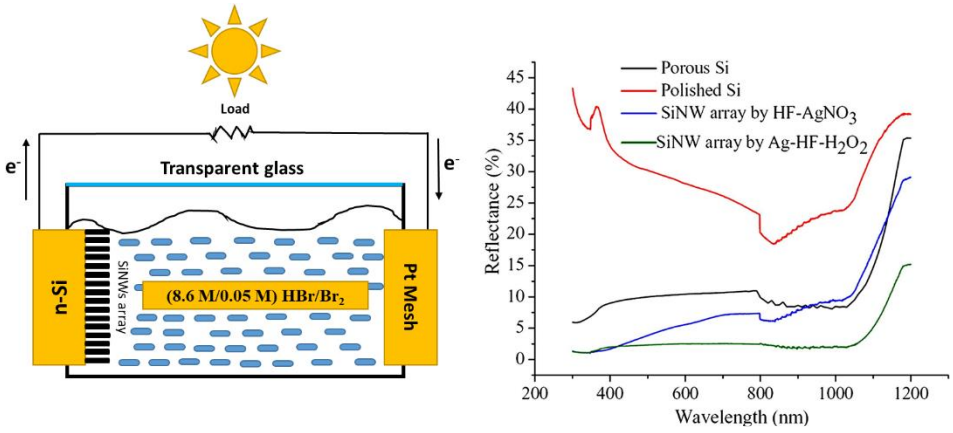

Figure 1.9.3. Cell structure and reflectance measurement of various photoelectrodes

advantage of using electroless etching is that there is no need for further doping, and also the obtained nanowires are much rougher as compared to nanowire grown using VLS and oxide assisted methods and hence have better ant reflectivity property. The redox electrolyte used in this case was (8.6 M/0.05 M) HBr/Br_2. The cell parameters obtained in this case were **V_{OC} = 0.73±0.02 V, J_{SC} = 0.872 mA/cm^2, FF = 0.45, PCE = 0.29%. [15]**

In 2009 Dalchiele et al. reported that nanorods array, which has limited carrier collection and low depletion region recombination, has improved performance as compared to planar Si substrate. It was also reported that the dark appearance of SiNW is not only the result of low reflectance but also due to anti reflectivity and light trapping effects. The open-circuit voltage was found to be higher in the case of planar n-Si because photogenerated minority carriers are distributed throughout the SiNW array; hence minority carrier flux across the junction interface will be less for SiNW. The other factors such as J_{sc}, FF, and efficiency of SiNW is higher because of antireflective ability, better collection of minority carrier, and the improved ratio of charge transfer relative to the junction recombination. The electrolyte used in this case was 0.5 M KNO_3 + 0.1 M $K_3Fe(CN)_6$ + 0.1 M $K_4Fe(CN)_6$ solution, and the cell was the three-electrode system with the counter electrode and SCE as the reference electrode. **[16]**

TABLE 2: Averaged PEC J-E data for clean polished n-Si and n-SiNW array electrodes in 0.1/0.1 M $[Fe(CN)_6]^{4-/3-}$ redox electrolyte under white illumination, 40 mW/cm^2.

Electrode	V_{oc}(mV)	J_{sc}(mA/cm^2)	Fill Factor	Efficiency
Clean polished n-Si	390±10	0.75±0.05	0.21±0.06	0.15±0.06
n-SiNW	323±10	0.89±0.05	0.41±0.06	0.30±0.06

In 2009 Peng et al. tried to overcome the major barriers to achieve highly efficient solar cell, i.e., junction recombination and poor carrier collection. So, SiNW decorated with PtNPs are reported, and it was found that with the increase in deposition time, the efficiency of the cell increases, and it was found that for about 25 min. of deposition, the efficiency of 8.14% was achieved, but further deposition of PtNPs led to decrease inefficiency, and this decrease can

be explained on the basis of series resistance that initially the deposited PtNPs decreases the series resistance which increases the fill factor and hence efficiency, but when there is prolonged deposition then there is the formation of porous Si layer which increases series resistance and hence the fill factor as well as efficiency decreases. The electrolyte used was (8.6 M/0.05 M) HBr/Br_2 with Pt mesh as the counter electrode. The cell parameters obtained were **V_{OC} = 0.58 V, J_{SC} = 17.2 mA/ cm^2, FF = 0.61, PCE = 6.1%. [17]**

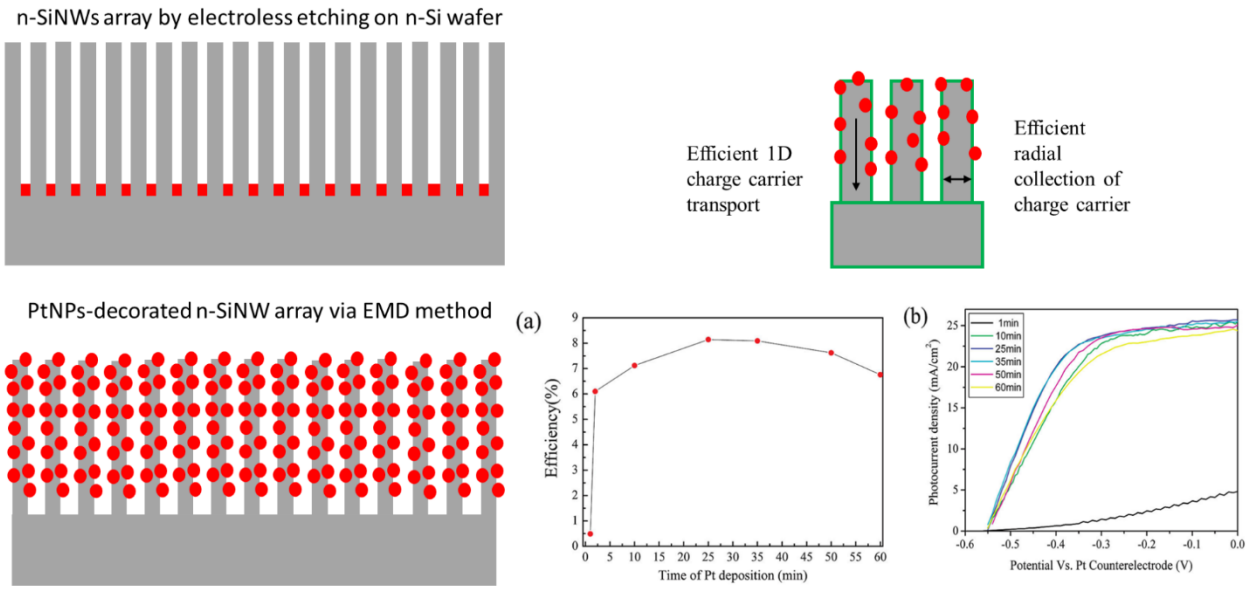

Figure 1.9.4. Structure of PtNPs decorated SiNW showing 1D charge transport and radial collection; (a). change in efficiency with PtNPs deposition time, (b). Change in photocurrent with time

In 2010, Shen et al. reported the combination of Ionic liquid along with $–CH_3$ termination and Pt nanodots decorated onto SiNW array as shown below and redox electrolyte used in this case was Iodine/Iodide along with counter electrode ITO and the cell parameters reported in this work were **@50 mW cm^{-2}, J_{sc} = 23.2 mA cm^{-2}, V_{oc} = 0.322 V, FF = 0.40, PCE = 6.0%**. The cell was tested using various electrodes such as Planar Si-H, SiNW-H, SiNW-CH_3 and SiNW-CH_3(Pt), and it was found that the SiNW-CH_3(Pt) electrode has better performance because methylation passivates the dangling Si bonds hence suppresses charge recombination and reduces current leakage due to insulating properties and platinum nanodots act as a catalyst

and hence helps increasing photocurrent. The ionic liquid used helps in obtaining low viscosity electrolyte also acts as a better solvent for the redox electrolyte. **[32]**

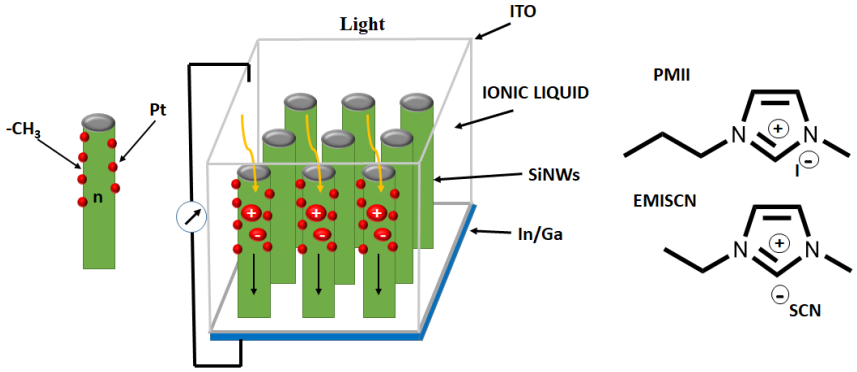

Figure 1.9.5. Schematic drawing of the PEC cell structure using SiNW as an electrode, molecular structures of ILs utilized for PEC cell is shown.

In 2011, Peng et al. reported PtNPs@C@SiNW (the figure is shown below), and it leads to better performance of the photoelectrochemical cell. The improved performance of the cell is due to the passivating effect of carbon fabric over SiNW as it helps in suppressing charge recombination and also helps to avoid photo corrosion and photooxidation of SiNW another advantage of doing carbon coating is that it is environmentally friendly and chemically stable. The pumps used also helps in the enhancement of cell performance because of their catalytic property towards redox electrolyte used in this case, i.e. (8.6 M/0.05 M) HBr/Br_2, and the counter electrode was Pt mesh. The cell parameters obtained in this case were **V_{OC} = 0.53 V, J_{SC} = 36.89 mA/ cm^2, FF = 0.55, PCE = 10.86%. [33]**

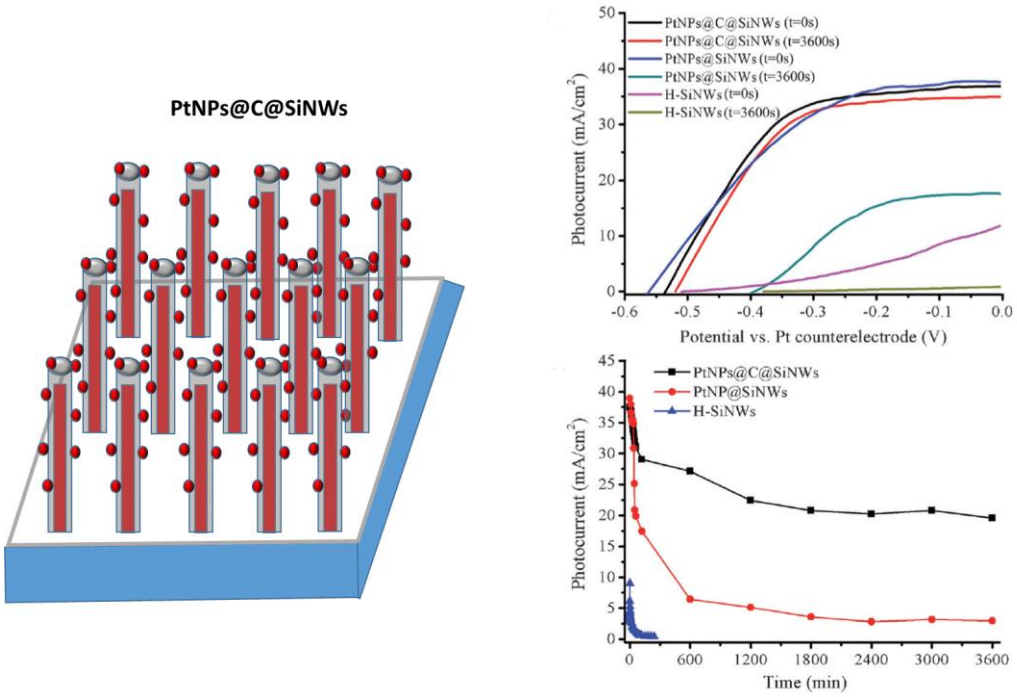

Figure 1.9.5. PtNPs decorated SiNW, graphs showing the change of photocurrent with the time of various electrodes

The major problems that come underway when SiNW are used are poor front electrode contact, the electrode can only be printed on the tips of SiNW, the shrinkage of contact area increases contact resistance, and it is difficult to realize good lateral carrier transport. In 2016 Jia et al. tried to overcome these problems by growing ZnO NRs between the SiNW. The growth of ZnO NRs led to the mutual connection between them and hence provided a channel for lateral carrier transport. The change in cell parameters with the introduction of ZnO NRs is shown below, along with cell configuration. **[34]**

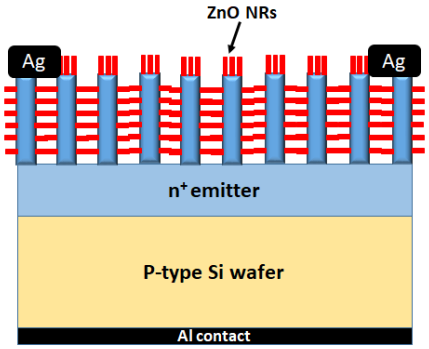

Figure 1.9.6. SiNW with ZnO nanorods grown between them.

TABLE 3. The current density-voltage (J-V) characteristics of the Si NW solar cells with and without ZnO NRs were measured under Standard Test Condition (AM 1.5 irradiation, T=300 K and 1 kW/m^2)

PROPERTY	SiNWs	SiNWs + ZnO NRs
J_{SC} (mA/cm^2)	22.5	27.9
FF	56.3	67.7
Efficiency(%)	9.2	10.8

In 2019, Rui et al. passivated the SiNW with Diallyl Disulfide (DADS), and high PCE was obtained due to the formation of Si-C bonds there is an improvement in PCE as well as stability of PV devices. This can be predicted from the graph shown below as we can see that as the time passes the J-V curve, the shape of H-terminated SiNW changes and become S-shaped, but the DADS terminated SiNW curve remains stable. The PCE of the H-terminated SiNW deteriorates faster than DADS-terminated SiNW. The cell parameters obtained in this case were **V_{oc} = 488 mV, J_{sc} = 28.8 mA/cm^2, FF = 49.0%, PCE = 7.02%. [35]**

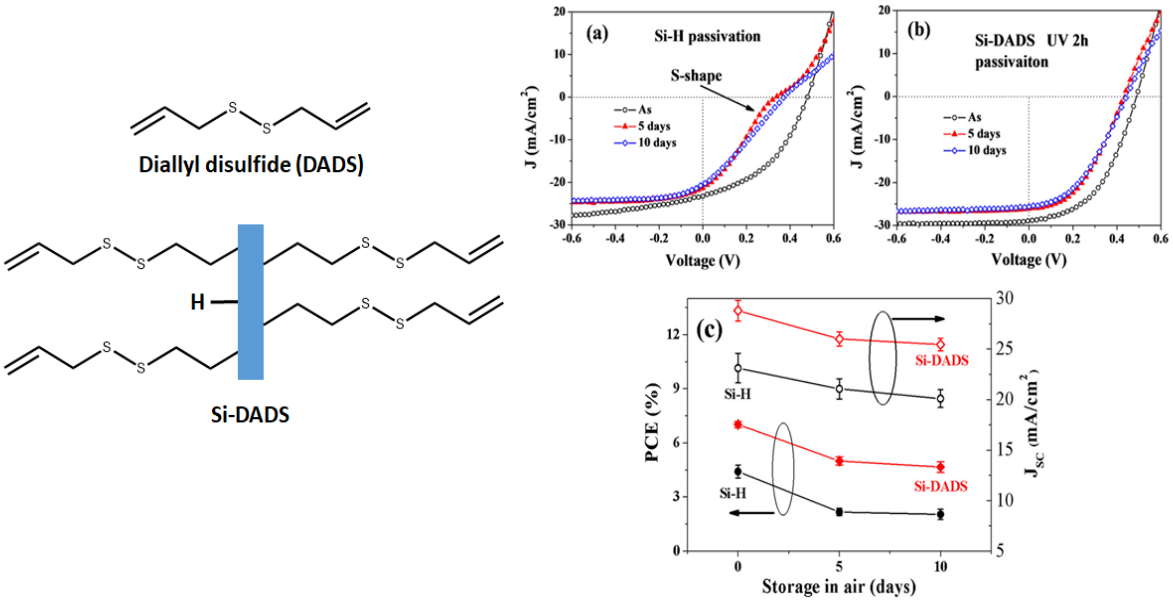

Figure 1.9.7. Structure of DADS molecule, SiNW decorated with DADS, Graphs showing the change in current density and PCE with time.

In 2019 Kolay et al. decorated SiNW with trigonal selenium particles in liquid junction photoelectrochemical cell and was investigated; the counter electrode used in this case was C-fabric due to its properties such as low sheet resistance, high surface area (mesh-like morphology), good stability in low pH, superior wettability and conductance helps to improve

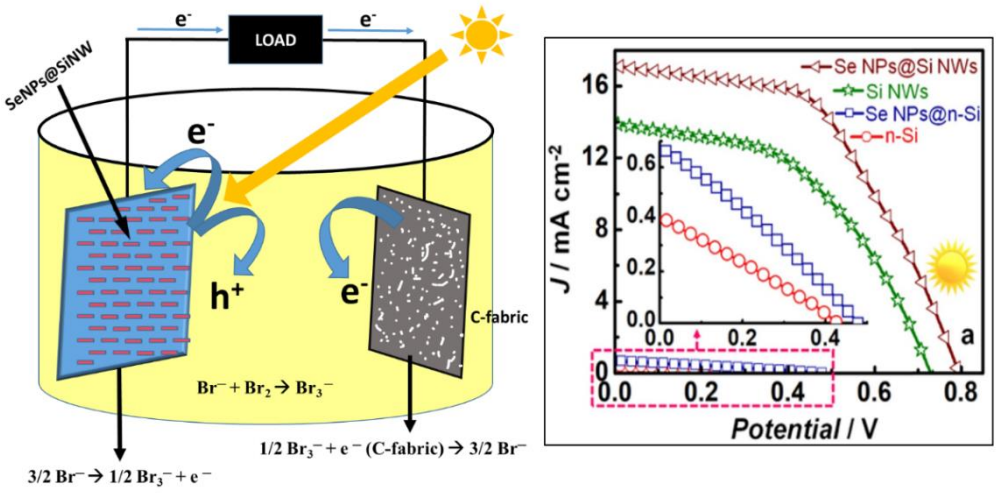

Figure 1.9.8: Cell structure with SeNPs decorated SiNW immersed in redox electrolyte, the graph shows J-V characteristic of various Photoelectrode.

The performance of the cell. The redox electrolyte used in this case was bromine/bromide-based electrolyte, i.e. (8.6 M/0.05 M) HBr/Br_2. The use of SeNPs also helps in improving the performance of the cell due to its well-positioned HOMO orbital, which lies above the HOMO of SiNW due to which it acts as a very efficient hole conductor and increases the recombination resistance, also due to its particle size it helps in scattering the light into far-field and hence increases the effective path length. The cell parameters obtained in this case were **V_{OC} = 0.79 V, J_{SC} = 17.12 mA/cm^2, FF = 0.52, PCE = 7.03%. [36]**

In 2019 again, Kolay et al. decorated SiNW with C@TeNRs over SiNW to improve the cell performance; due to efficient charge transfer properties of TeNRs, the PCE of the solar cell increases. The C@TeNRs layer that is affixed to the axial length of SiNW helps to passivate the surface and helps to protect against photo corrosion and photooxidation. As the HOMO of TeNRs lies above the HOMO of SiNW hence, it helps in rapid hole injection from SiNW to redox electrolyte, i.e. (8.6 M/0.05 M) HBr/Br_2. The counter electrode used in this cell was C-fabric and cell parameters obtained are **V_{OC} = 0.89 V, J_{SC} = 23.3 mA/cm^2, FF = 0.56, PCE = 11.5 ± 0.1%. [37]**

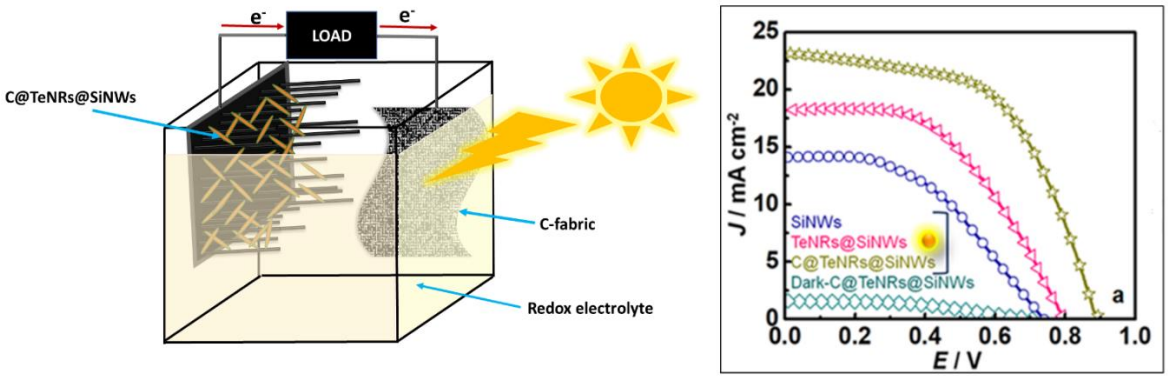

Figure 1.9.9. C@TeNRs@SiNW cell structure immersed in redox electrolyte, the graph showing the J-V characteristic of various Photoelectrode.

In a recently published article in 2020, Seo et al. used Hour-Glass shaped SiNW (HG-SiNW) in place of cylindrical nanowires (C-SiNW), and it was found that the J_{sc} increased by about 1.85

times in the case of HG-SiNW as compared to C-SiNW which leads to the higher efficiency of the solar cell. The reduced surface area in the case of HG-SiNW is responsible for the high PCE because it reduces surface recombination, and hence it increases the fill factor. The induced repeated total reflection due to tapering of the upper part of HG-SiNW led to the increase in the trapping of light. The V_{OC} remains almost the same, but there is an increase in J_{sc} and FF, as shown below. **[38]**

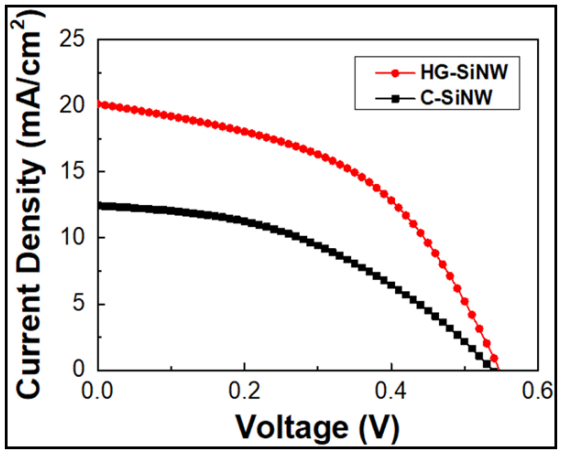

Figure 1.9.10. J-V curve of HG-SiNW and C-SiNW.

TABLE 4: Measured J–V characteristics of both solar cells under AM 1.5G illumination with 100 mW/cm^2

Type	V_{oc}(V)	J_{sc}(mA/cm^2)	FF(%)
HG-SiNWs	0.55	20.12	47.49
C-SiNWs	0.54	12.44	42.44

In 1984 Lewis et al. tried to observe the variation of open-circuit voltage (V_{oc}) with the change in majority carrier concentration (N_D), minority carrier diffusion length (L_P), and cell temperature.

The cell setup used in this case was **ELECTRODE: n-Si** (10s etch in 49% HF and washed in CH_3OH); **ELECTROLYTE:** 0.2 M (1-hydroxyethyl) Fc/0.5 mM (1-hydroxyethyl) Fc^+/1.5 M $LiClO_4/CH_3OH$ **Voc:** 0.55-0.56 V, **Jsc:** 20 mA/cm^2. Firstly, he kept diffusion length constant and varied majority carrier concentration and obtained large variation in V_{oc}. With the degradation in hole lifetime, there is a substantial decrease in V_{oc}. From the above two results, he concluded that the bulk recombination and diffusion effects dominate the V_{oc} at n-Si/CH_3OH interface. It was also found that the V_{oc} decreased linearly with an increase in temperature. Further, in studies, it was found that the growth of Silicon oxide was the factor in the improvement in cell performance because silicon oxide has a passivating effect. The cell parameters obtained in this case was **mirror-finished n-Si wafer**: Efficiency = 10.0% ± 1.0%; V_{OC} = 0.62-0.63 V; J_{SC} = 19-20mA/cm^2; **matte etched n-Si wafer**: Efficiency = 12.0% ± 1.5%; V_{SC} = 0.62-0.64 V, J_{SC} = 22-24mA/cm^2. **[40]**

Table 5: Variation in open-circuit voltage of n-Si/CH_3OH junctions.

Resistivity ρ (Ω cm)	Wafer thickness W (μm)	Hole diffusion length L_P (μm)	V_{OC} (theory) (V)	V_{OC}(exptl) (V)
0.20	315	195	0.630	0.630
0.60	370	165	0.589	0.593
1.50	390	190	0.566	0.568
1.95	330	85	0.540	0.550
1.70	240	45	0.528	0.523
1.70	240	12	0.492	0.495
1.70	240	8	0.482	0.470
1.70	240	5	0.470	0.462

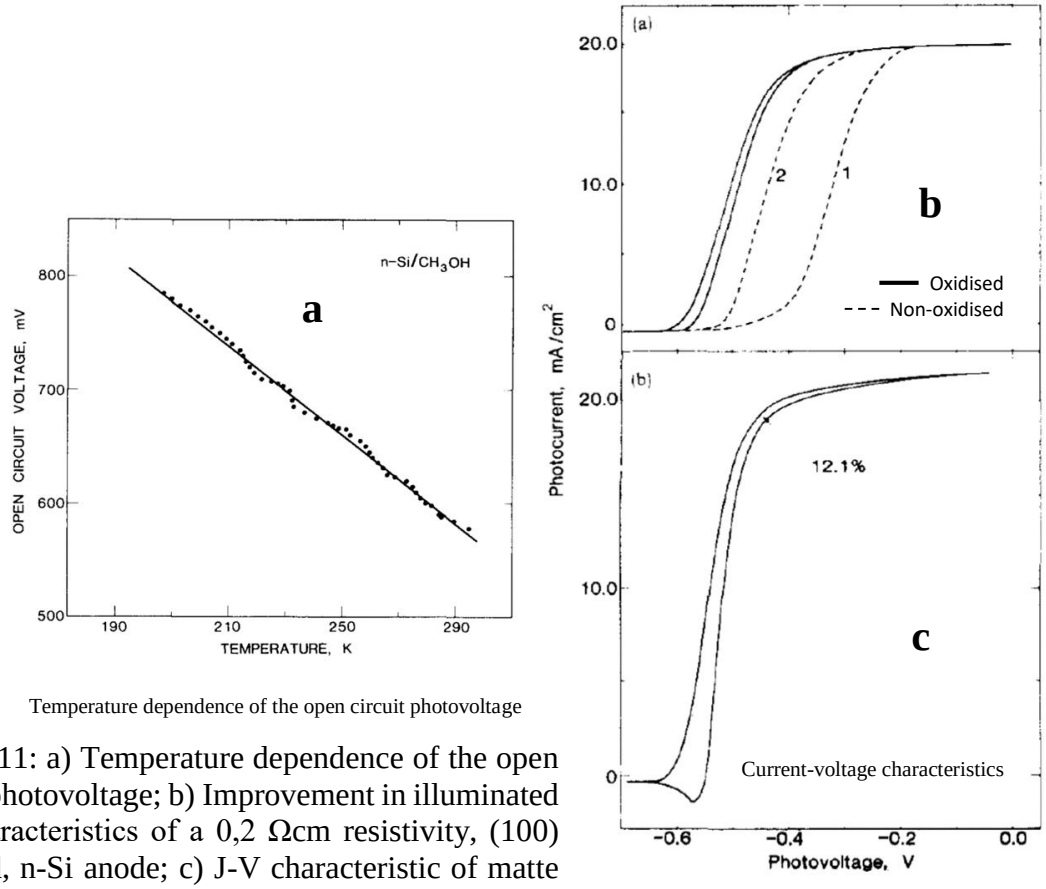

Temperature dependence of the open circuit photovoltage

Fig 1.9.11: a) Temperature dependence of the open circuit photovoltage; b) Improvement in illuminated J-V characteristics of a 0,2 Ωcm resistivity, (100) oriented, n-Si anode; c) J-V characteristic of matte textured n-Si.

In 1984 Lieber et al. carried study to find evidence against surface state limitations on the efficiency of p-Si/CH_3CN junction, the electrolyte used in this case was 1.0M $[(C_2H_5)_4N]^+[BF_4]^-$ /0.2M $CoCp_2^+$/0.5mM $CoCp_2/CH_3CN$, mirror, and the matte-finished p-Si electrode was used as photoanode and Pt mesh as the counter electrode. It was observed that there was no significant photocurrent near the absorption edge, which implies that the charge carriers which are unthermalized do not participate in current at p-Si/CH_3OH interface. It was also found that as the light intensity increased the V_{oc} of p-Si/CH_3OH exceeds the V_{oc} of p-Si Schottky barriers of metals such as Cr, Cu, Ni and W. the cell parameters obtained in this cell were **Mirror finished p-Si electrode**: V_{OC} = 0.48-0.52 V; J_{SC} = 20-21 mA/cm$^{2;}$ Fill factor = 0.52-0.55; PCE = 8.5 ± 1.0%; **Matte p-Si electrode**: V_{OC} = 0.49-0.53 V; J_{SC} = 23-26 mA/cm^2; PCE = 10.5 ± 1.0%. **[41]**

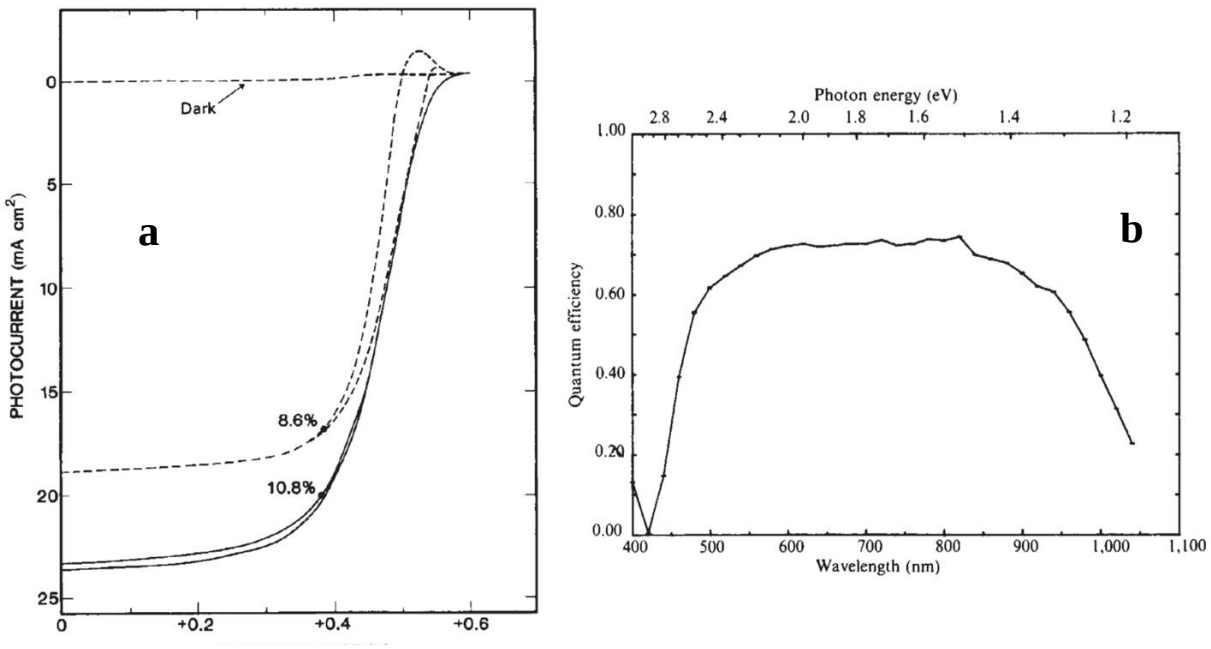

Fig 1.9.12: a) J-V characteristic of a single crystal p-Si photocathode; b) Spectral response

In 1986 Green et al. reported the kinetic transport studies of carrier recombination at Si/liquid interface. Many electrolytes such as [$MV^{2+/+}$ (MV = N/N'-dimethyl-4,4'-bipyridinium), $BV^{2+/+}$ (BV = N, N'-dibenzyl-4,4'bipyridinium), $Fc^{+/0}$ (Fc = Ferrocene), $AcFc^{+/0}$ (AcFc = acetylferrocene),

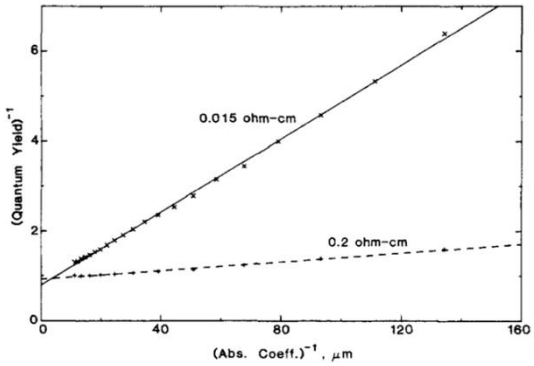

Fig 1.9.13: Natural logarithm of the short-circuit photocurrent density vs. the open-circuit photovoltage

$TMPD^{+/0}$ (TMPD = N, N, N', N'-tetramethylphenylenedi-amine), $Me_2Fc^{+/0}$ (1,1 '-dimethyl ferrocene), $CoCp_2^{+/0}$ (cobaltocene), and $Me_{10}Fc^{+/0}$ (bis(pentamethylcyclopentadienyl)iron)] were used in the cell in nitrogen atmosphere. From the spectral response of cells in the range 800-1100 nm, the diffusion length can be measured. The graph plotted between the inverse of quantum yield and absorption coefficient and the intercept on abscissa yielded the value of diffusion length. It was also observed that the diffusion length is directly proportional to the resistivity of the wafer. With the decrease in resistivity, the V_{oc} also decreases; hence there exists an optimum dopant

density for better photovoltaic response at the Si/liquid interface. With the temperature change, there was no substantial change in photocurrent observed. Observations also found that change in concentration has a negligible impact on open-circuit voltage. **[42]**

Resistivity, Ω-cm	L_p, µm	V_{OC}(theory), mV	V_{OC}(exptl), mV	V_{OC}(0.0 K), V	Temp. variation mV/K(Theory)	Temp. variation mV/K(exptl)
1.5	190	568	565	1.20	2.11	2.20 ± 0.10
0.6	165	592	593	1.20	2.03	2.0 ± 0.05
0.2	195	635	635	1.22	1.89	1.94 ± 0.05
0.015	17	670	670	1.21	1.76	1.80 ± 0.05
0.0025	1	579	579	-	2.07	-

Table 6: Transport Data for the n-Si/$Me_2Fc^{+/0}$-$LiClO_4$-CH_3OH Interfaces

Entry	[Me2Fc], M	[Me2Fc]+, M	V_{OC}, mV
1	0.20	0.0010	641
2	0.20	0.0050	642
3	0.20	0.0100	643
4	0.10	0.0050	643
5	0.010	0.0005	645

Table 7: Effect of Concentration on V_{oc}

In 2007 Maiolo III et al. investigated a high aspect ratio silicon wire array as photoanode in a photoelectrochemical cell. To absorb 90% of the energy from sunlight, a Si wafer of about 100 µm is required, so an alternative for this is to use a wire array with sufficient length to absorb the light axially and have a small diameter to facilitate efficient and radial collection of carriers. In theoretical treatment, it was found that optimal efficiency is expected when the diameter of the wires is comparable to minority carrier diffusion length. The cell configuration used in this case was **ELECTROLYTE**: 1,1'-dimethyl Ferrocene (Me_2Fc) $^{+/0}$ redox system in CH_3OH, **PHOTOANODE**: n-SiNW, **COUNTER ELECTRODE**: Pt. The fill factor obtained in this cell was low, which was due to recombination at the junction and can be improved through surface passivation. **[43]**

Table 8: Photocurrent and Photovoltage of Wire Array Cells

Photoanode	V_{OC}(mV)	J_{SC}(mA/cm^2)
Wire array	389 ± 18	1.43 ± 0.14
Control(no wires	232 ± 8	0.28 ± 0.01

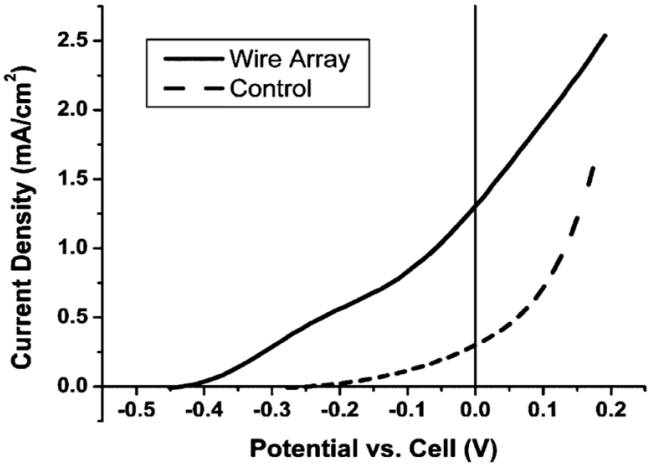

Fig 1.9.14: Current density versus voltage behavior for a Si wire array (solid) and control samples (dashed)

In 2008 Maiolo et al. used macroporous silicon as a photoanode in SiNW solar cells; the cell configuration used in this case was **ELECTROLYTE**: 1,1'-dimethylferrocenenium/Ferrocene ($Me_2Fc^{+/0}$) redox couple in CH_3OH; **COUNTER ELECTRODE**: Pt mesh; **WORKING ELECTRODE**: Macroporous Si. It was found that pore length was dependent on etching time, whereas the diameter was independent of etching time. The J_{sc} in the case of macroporous silicon was lower as compared to planar silicon, but the J_{sc} was independent of pore length. The PCE of the planar Si cell was 14%, and that of macroporous Si is 10-12%. The low value of V_{oc} in macroporous Si is due to lower minority carrier flux. **[44]**

Etch time	V_{OC}(mV)	J_{SC}(mA/cm^2)	Fill factor(%)	Efficiency(%)
Planar(100)	566 ± 2	36.4 ± 2.6	70.3 ± 1.4	14.4 ± 0.9
15 min	552 ± 3	32.6 ± 2.0	69.1 ± 2.0	12.2 ± 0.7
30 min	543 ± 3	30.7 ± 1.2	68.9 ± 3.1	11.4 ± 0.5
45 min	517 ± 8	30.7 ± 1.4	64.7 ± 1.9	10.2 ± 0.5
60 min	485 ± 12	34.0 ± 2.0	63.9 ± 1.8	10.6 ± 0.8
Planar(110)	601 ± 2	32.1 ± 1.1	73.7 ± 2.9	14.2 ± 0.4

Table 9: Figures of Merit

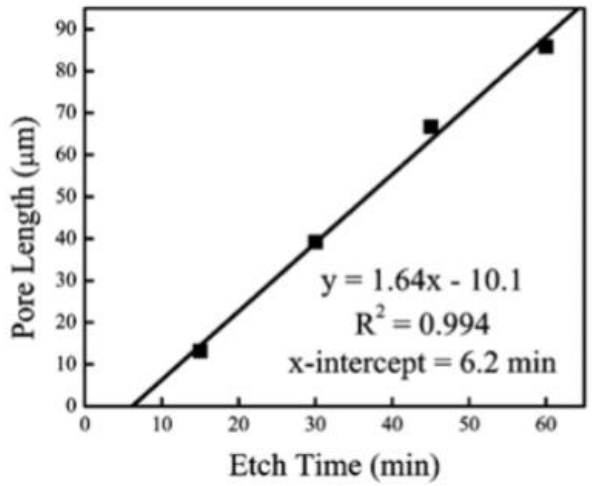

Fig 1.9.15: Plot of pore length vs. etch time. The growth rate was~1.6 μm min $^{-1}$, with pore initiation time of~6

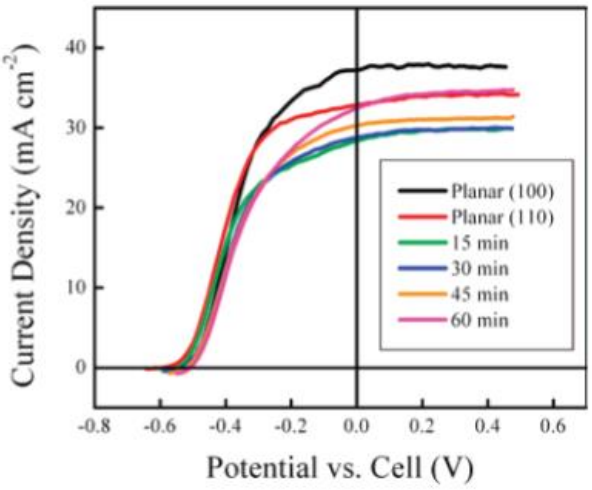

Fig 1.9.16: J-E data at 10 mV s^{-1} under 100 mW cm^{-2} of illumination

In 1983 Gronet et al. n-type silicon was used in methanol led to a 10.1% efficient semiconductor/liquid junction solar cell. The cell configuration used was **ELECTROLYTE**: 0.2M (1-hydroxyethyl) Ferrocene, 0.5 mM (1-hydroxyethyl) ferricenium, and 1.0 M $LiClO_4$; **PHOTOANODE**: n-Type Si electrodes; **COUNTER ELECTRODE**: Pt. The non-aqueous medium helps to suppress the corrosion at semiconductor photoanode. The main problems faced were recombination sites are present at the surface also thermionic emission led to a large value of

Table 10: Representative conversion efficiencies for optical energy

Input (mW/cm²)	Quantum yield	V_{OC}	V_{pmax}	Efficiency(%)
2.20	0.70	0.44	0.34	9.6
3.76	0.65	0.46	0.36	9.9
7.53	0.60	0.48	0.34	8.9
11.1	0.63	0.50	0.34	9.5
15.1	0.62	0.51	0.34	9.2
18.1	0.64	0.52	0.34	9.7

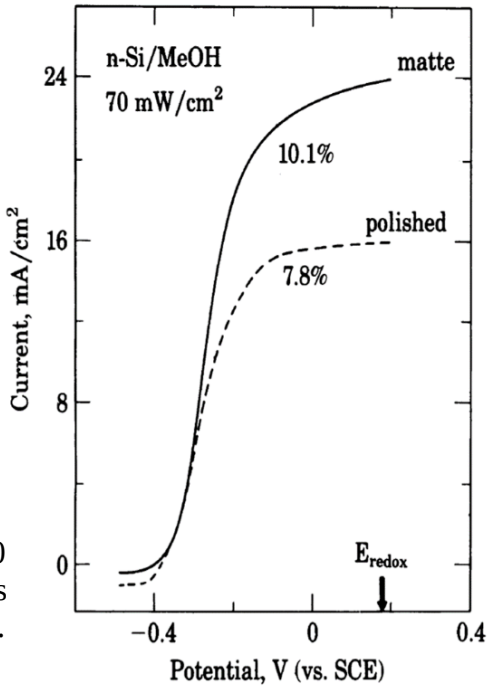

Fig 1.9.17: Current-voltage characteristics (50 mV/sec) of (100) oriented n-type Si electrodes in 1.0M$LiClO_4$/MeOH with 0.2MI, 0.5mM I^+.

dark current. The solution suggested was to chemically treat the surface, which reduces the recombination sites on the surface through passivation. The result obtained for plane Si substrate was **V_{OC} = 0.53 V, J_{SC} = 17 mA/cm^2, FF = 0.60, PCE = 7.8%** and that for matte etched sample was **V_{OC} = O.53 V, J_{SC} = 22.2 mA/cm^2, FF = 0.59, PCE = 10.1%**. **[45]**

Table 11: Solar cell parameters of liquid junction Si NWs based solar cells reported in the literature.

Cell	**V_{OC} (V)**	**J_{SC} (mA cm^{-2})**	**FF**	**PCE (%)**	**Reference**
Anode: Planar silicon **CE:** ITO **Electrolyte:** 0.15-0.2 M 1, 1'-dimethylferrocene/0.15-0.2 M 1, 1'-dimethylferricenium tetrafluoroborate/1.0 M lithiumperchlorate/methanol	0.60-0.61	28-34	0.69-0.77	14.0 ± 1.0	[13]
Anode: Methyl terminated SiNW **CE:** Pt **Electrolyte:** $[Fe(CN)6]^{3-/4-}$	0.42-0.48	----	0.57-0.64	-----	[14]
Anode: n-SiNW **CE:** Pt Mesh **Electrolyte:** 8.6 M/0.05 M HBr/Br_2	0.73±0.02	0.872	0.45	0.29	[15]
Anode: n-SiNW **CE:** Pt **Reference Electrode:** SCE	0.323±0.1	0.89±0.05	0.41±0.06	0.30±0.06	[16]

Electrolyte: 0.5 M KNO_3 + 0.1 M $K_3Fe(CN)_6$ + 0.1 M $K_4Fe(CN)_6$					
Anode: PtNPs@SiNW **CE:** Pt Mesh **Electrolyte:** 8.6 M/0.05 M HBr/Br_2	0.58	17.2	0.61	6.1	[17]
Anode: Methyl terminated SiNW decorated with Pt nanodots **CE:** ITO **Electrolyte:** I^-/I_3^-	0.322	23.2	0.40	6.0	[32]
Anode: PtNPs@C@SiNW **CE:** Pt Mesh **Electrolyte:** 8.6 M/0.05 M HBr/Br_2	0.53	36.89	0.55	10.86	[33]
Anode: n-SiNW with ZnO nanorods between them **CE:** Pt	----	27.9	0.677	10.8	[34]
Anode: Diallyl disulfide passivated SiNW **CE:** Ag grid	0.488	28.8	0.49	7.02	[35]
Anode: SeNPs@SiNW **CE:** C-fabric **Electrolyte:** 8.6 M/0.05 M HBr/Br_2	0.79	17.12	0.52	7.03	[36]
Anode: C@TeNRs@SiNW **CE:** C-fabric **Electrolyte:** 8.6 M/0.05 M HBr/Br_2	0.89	23.3	0.56	11.5 ± 0.1	[37]

Anode: Hour-glass shaped SiNW	0.55	20.12	0.47	----	[38]
Anode: matte etched n-Si wafer **CE:** Pt **Electrolyte:** 0.2 M (1-hydroxyethyl) Fc/0.5 mM (1-hydroxyethyl) Fc+/1.5 M $LiClO_4/CH_3OH$	0.62-0.64	22-24	----	12.0% ± 1.5	[39]
Anode: matte etched n-Si wafer **CE:** Pt **Electrolyte:** 1.0M $[(C_2H_5)_4N]+[BF_4]$-/0.2M $CoCp_2^+$/0.5mM $CoCp_2/CH_3CN$	0.49-0.53	23-26	----	10.5±1.0	[40]
Anode: n-SiNW **CE:** Pt **Electrolyte:** 1,1'-dimethylferrocene (Me2Fc) $^{+/0}$ redox system in CH_3OH	0.389±0.018	1.43±0.14	-----	----	[41]
Anode: Macroporous Si **CE:** Pt **Electrolyte:** 1,1' dimethylferrocenenium/Ferrocene ($Me_2Fc^{+/0}$) redox couple in CH_3OH	0.55-0.48	32.6-34	0.64-0.69	10.6-12.2	[42]
Anode: n-Si **CE:** Pt **Electrolyte:** 0.2M (1-hydroxyethyl) Ferrocene, 0.5 mM	0.53	22.2	0.59	10.1	[43]

(1-hydroxyethyl) ferricenium, and 1.0 M LiClO4					

2. Experimental

2.1 Chemicals

Silicon (n-type) wafers were acquired from Siegert wafer. Copper nitrate [$Cu(NO_3)_2 \cdot 3H_2O$], silver nitrate ($AgNO_3$), and PEI were purchased from Sigma Aldrich. Sulfuric acid (H_2SO_4, 98%), nitric acid (HNO_3, 69%), hydrogen peroxide (H_2O_2, 30%), hydrofluoric acid (HF, 40%), hydrobromic acid (HBr, 47%), formic acid (HCOOH, 99%), ethanol, and acetone were purchased from Merck. Bromine (Br_2) was bought from SDFCL. C-fabric was procured from Alibaba Pvt. Ltd and ultra-pure water with a resistivity of ~18.2 MΩ cm were obtained through a Millipore Direct–Q3 UV system.

2.2 Preparation of Cu_2O Microcrystals with Controlled Morphology:

Firstly, 724.8 mg of copper nitrate [$Cu(NO_3)_2 \cdot 3H_2O$] is mixed with 60 ml of ethanol to form 0.05 M copper nitrate solution. Then, in the prepared solution, 4 ml of formic acid is added. Then the prepared solution is sonicated in the water bath for 10 min. The above solution is then transferred to a Teflon-lined stainless steel autoclave. The autoclave was sealed tightly and heated at 150°C for 2 hrs. Then the vessel is cooled to room temperature naturally. The red powder is filtered, washed with distilled water and ethanol several times, and then dried at 60°C for 5 hrs. and the obtained product is further characterized using different techniques.

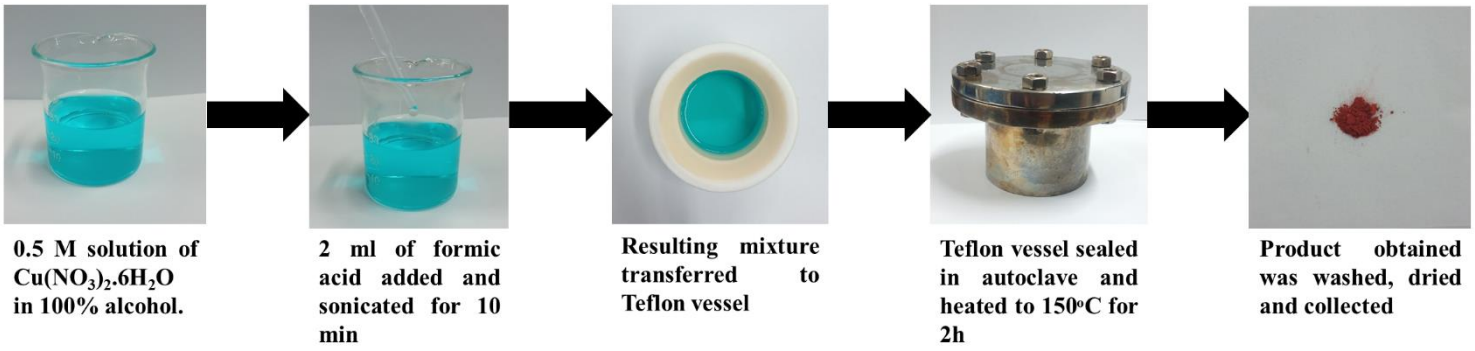

Fig 2.2: Preparation of Cu_2O

2.3 Etching: Metal Assisted Chemical Etching [46]

1. The n-type wafer is cleaned in acetone, IPA, and DI water, respectively, for 10 min each at room temperature.
2. Then the wafer is dipped into piranha solution, which consists of H_2SO_4 and H_2O_2 in a 3:1 ratio for 30 minutes to remove residues from the surface.
3. Then the wafer is immersed into an aqueous solution containing 5M HF and 0.02M $AgNO_3$ for 45 min.
4. SiNW are obtained with a thick silver dendritic coating.
5. The obtained sample is dipped in NH_4OH: H_2O_2 (3:1) solution to dissolve residual Silver, and we obtain black-colored vertically aligned SiNW.
6. The etched SiNW are then dipped into 5% HF solution for 1 min to obtain bundle free SiNW.

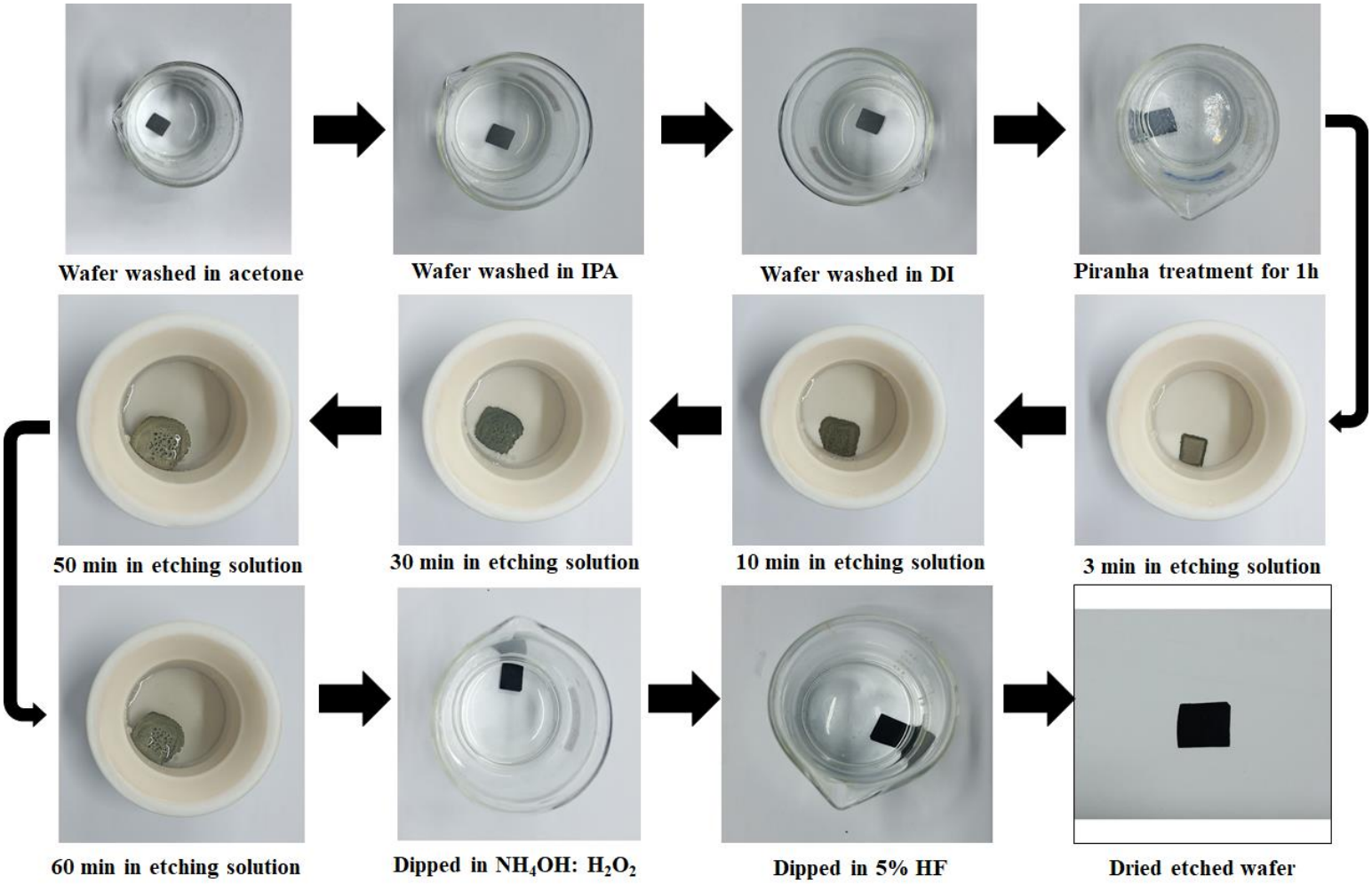

Fig 2.3.1: SiNW etching schematics

2.3.1 Mechanism of Etching [46]

2.3.1.1 Role of $AgNO_3$:

When the Si wafer is dipped in $AgNO_3$/HF solution, silver ions that are present in the solution extract an electron from the valence band of silicon. The extraction of electrons takes place because Silver is more electronegative than silicon. The silver ion gets reduced to Silver nuclei and gets deposited on the surface, which leads to the formation of a continuous Ag layer. Since the Ag extracts an electron from the Si surface, there is a formation of a hole in Si, which gets accumulated beneath the Ag layer.

2.3.1.2 Role of HF:

HF present in the solution reacts with oxidized Si to form water-soluble H_2SiF_6, due to which a fresh surface of Si comes in contact with the Ag catalyst, and further etching will take place in continuous a MaCE process.

2.3.1.3 Role of Piranha Pre-treatment:

Bundling of SINW on etching has been the major reason for the decrease in its performance. In 2014 Togonal et al. suggested a pre-treat wafer with piranha solution to obtain bundle-free nanowires. He pre-treated one wafer with 5% HF for 1 min. and another wafer with piranha solution and found that surface of the wafer treated with HF was hydrophobic, whereas the surface of the wafer treated with piranha was hydrophilic. The hydrophilic wafer surface resulted in the uniform deposition of Silver, and a uniformly etched wafer is obtained.

2.3.1.4 Role of 5% HF Post-treatment:

Trigonal et al. showed that the post-treatment of etched SiNW with 5% HF makes the surface hydrophobic, and hydrogen-terminated nanowires are obtained, and repulsion between nanowires helps to avoid agglomeration.

2.3.1.5 Reactions involved:

$$Ag^+ + e^- \rightarrow Ag \text{ (Cathode)}$$

$$Si + 6HF \rightarrow SiF_6^{2-} + 4e^- + 6H^+ \text{ (Anode)}$$

$$Si + 6HF + 4Ag^+ \rightarrow SiF_6^{2-} + 4Ag + 6H^+ \text{ (Overall)}$$

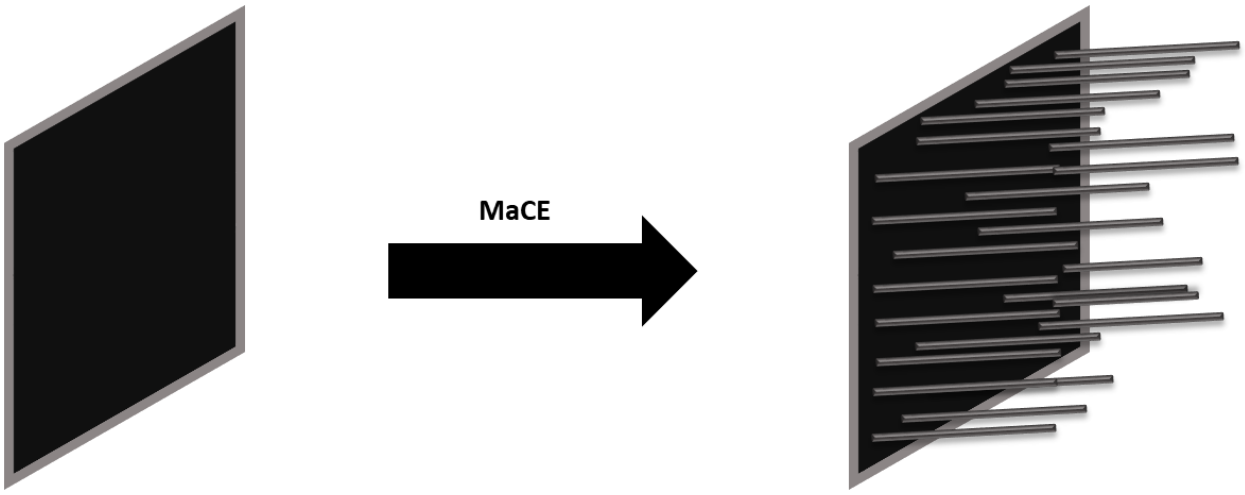

Fig 2.3.2: Si wafer before and after etching

2.4 Photovoltaic device fabrication:

The prepared Cu_2O microcrystals are dispersed in ethanol and then are decorated over SiNW using the drop-casting technique and then PEI polymer is coated over the Cu_2O@SiNW using spin coating technique to get the photoanode for the cell. C-fabric is chosen as a counter electrode due to its high conductivity and stability in the electrolyte. The electrolyte comprised 8.6 M HBr and 0.05 M Br_2 as the redox mix.

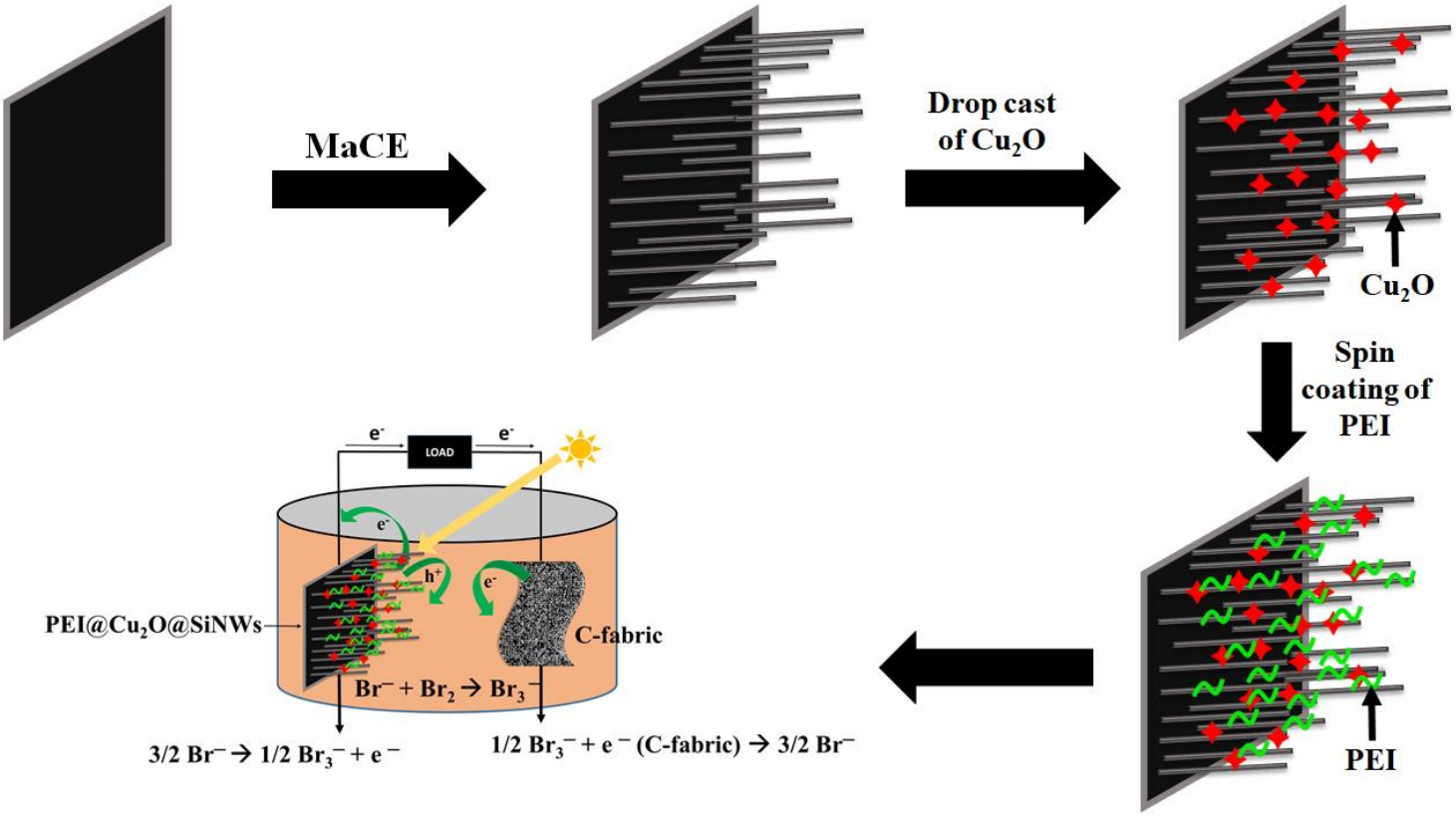

Fig 2.4: Cell fabrication scheme

3. Result and discussion

3.1 Structural Characterization

3.1.1 XRD Analysis

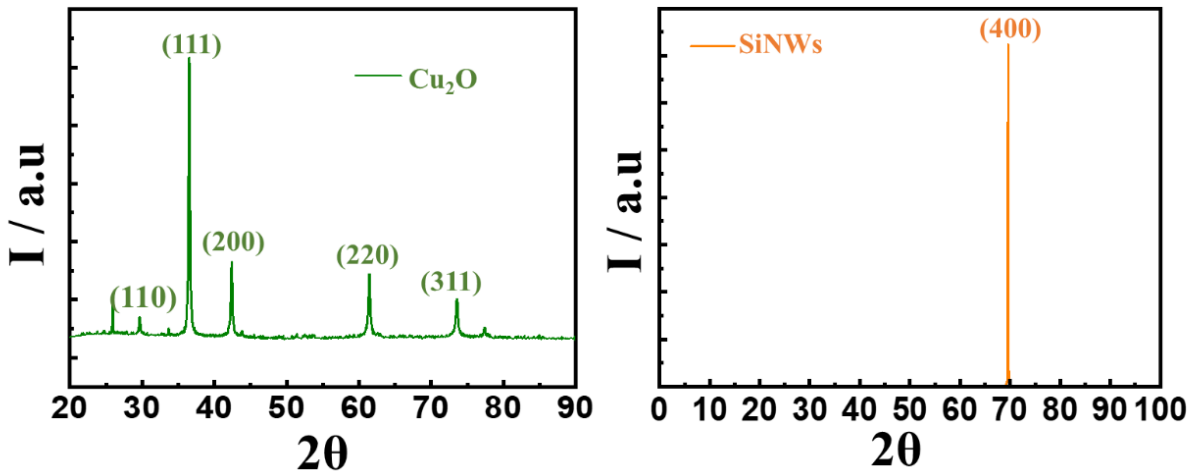

XRD peak positions obtained are in good agreement with Cu_2O nanoparticles obtained from The International Center of Diffraction Data card, conforming to Cuprous oxide nanoparticles' formation. The peaks obtained with 2θ values 29.78°, 36.56°, 42.36°, 61.44°, and 73.53° corresponds to the crystal planes (110), (111), (200), (220), and (311) respectively. The highly intense peak at 2θ = 69.5 and d = 1.36 Å corresponding to plane (400) parallel to (100) plane of the face-centered cubic (FCC) crystal lattice (JCPDS: 892955) of an n-Si wafer. [47]

3.2 Electrochemical characterization

3.2.1 Cyclic voltammetry

Cyclic voltammetry (CV) was performed under a three-electrode system with Pt as the CE and Ag/AgCl/KCl used as a reference electrode in an aqueous 0.1 M KCl electrolyte solution on an Autolab PGSTAT 302N equipped with a NOVA 1.9 software at a scan rate of 20 mV s-1. In the case of Cu_2O, an oxidation peak is observed in the anodic sweep, whereas in the case of SiNW, a reduction peak is obtained during the cathodic sweep. Since in the case of Cu_2O, we got the oxidation peak so we can equate it to HOMO or conduction band of Cu_2O, whereas in the case of SiNW, we obtained the reduction peak so it can be equated to LUMO or valence band. The electrochemical bandgap of SiNW and Cu_2O reported in the literature is 1.1 [36] and 2.17 eV [47]. The reference electrode has a potential of 0.197 V and is added to $E_{red.}$ vs. Ag/AgCl/KCl to get the E_{red} vs. normal hydrogen electrode(NHE) of the working electrode, the obtained value of E_{red} vs. NHE is subtracted from -4.5 eV (≡ 0 V vs. NHE) to convert the value to eV. The values of band positions obtained are summarized below in the table.

Equations used to calculate the band positions of Cu_2O and SiNW are given below:

$$Ered = -4.5\ eV\ (\equiv 0\ V\ versus\ NHE) - (Red.\ Peak\ (V)\ vs.\ Ag/AgCl/KCl + 0.197\ V)$$

$$Eox = -4.5\ eV\ (\equiv 0\ V\ versus\ NHE) - (Ox.\ Peak\ (V)\ vs.\ Ag/AgCl/KCl + 0.197\ V)$$

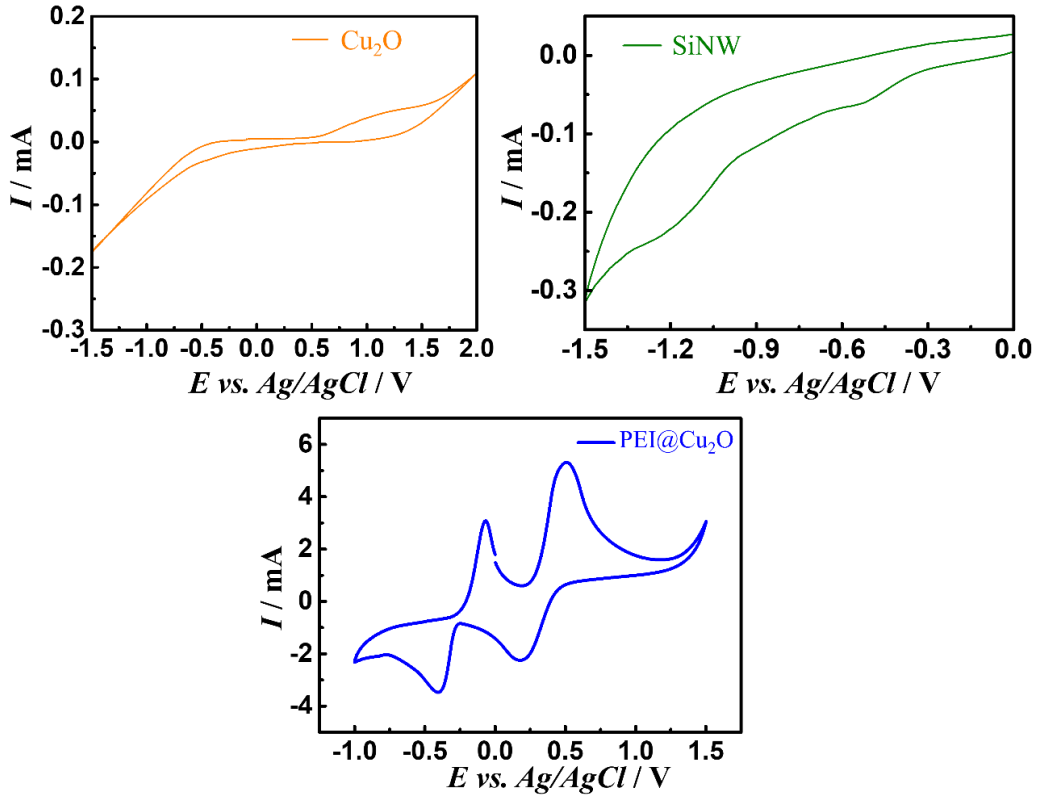

Fig 3.2.1. Cyclic voltammograms of a) Cu_2O; b) SiNW; c) PEI@Cu_2O

Table 12: Energy level positions of the photoanode

Material	Reduction peak/ V vs. Ag/AgCl	Oxidation peak / V vs. Ag/AgCl	Ered (versus NHE) / eV ≡ LUMO	Band Gap / eV	Eox (versus NHE) / eV ≡ HOMO
Cu_2O	-----	1.0	-3.43	2.17	-5.69
SiNW	-0.53	-----	-4.16	1.10	-5.26
PEI@Cu_2O	----	0.50	-3.02	2.17	-5.19

3.3 Solar Cell Performance:

3.3.1 J-V Diagram:

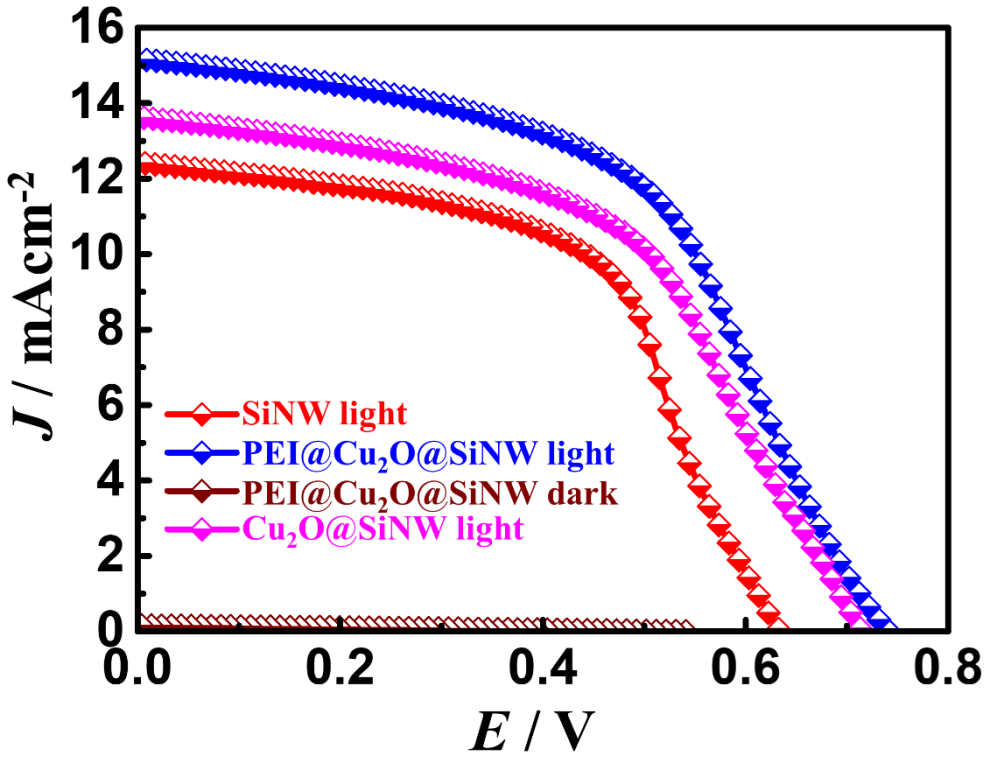

Fig 3.3.1. J-V plots of SiNW and PEI@Cu_2O@SiNW photoanode based liquid junction solar cell having C fabric as counter electrode and aqueous 8.6 M HBr and 0.05 Br_2 as electrolyte under illuminated (1 sun) and dark conditions.

Table 13: Solar cell parameters of liquid junction solar cells having different photoanodes under 1 sun illuminated condition.

Photoanode	**V_{OC} (V)**	**J_{SC} (mA cm^{-2})**	**FF**	**Efficiency(%)**
PEI@Cu_2O@SiNW(Dark)	0.54	0.16	0.26	0.023
SiNW (Light)	0.63	12.58	0.63	5.04
Cu_2O@SiNW (light)	0.71	13.62	0.52	5.08
PEI@Cu_2O@SiNW (Light)	0.74	15.16	0.68	7.65

Current versus potential (I−V) data of solar cells were measured using a LOT-Oriel solar simulator coupled with a Metrohm Autolab PSTAT302N. The light source was a 150 W Xenon arc lamp, which delivered a collimated output beam of 25 mm diameter through Air Mass (AM) 1.5 filter, providing a light intensity of 100 mW cm-2 (1 sun). From the plot shown above, we can see that in the case of PEI@Cu_2O@SiNW in the dark, the efficiency obtained is 0.023%. In the case of SiNW, the efficiency is 5.04%. This efficiency is attributed to the light trapping effect of SiNW; when SiNW is decorated with Cu_2O microcrystals, we obtain an efficiency of 5.08%, which is almost the same as SiNW this can be explained by the fact that HOMO of Cu_2O does not properly align to act as hole conductor also when the SiNW are decorated with Cu_2O microcrystals by drop-casting and further coated with PEI polymer the efficiency of the cell increases to 7.65% this increase in efficiency is attributed to property of PEI polymer which decreases the work function [48] of Cu_2O microcrystals and due to which the LUMO of Cu_2O lies above the LUMO of SiNW due to which it acts as hole transporting layer and increases the recombination resistance at SiNW/electrolyte interface.

3.3.2 Impedance studies:

Impedance measurements were performed on Autolab PGSTAT 302N. The Nyquist plots were generated over a frequency range of 1 MHz to 0.01 Hz by applying an ac potential of 20 mV over

the open circuit potential in the dark. In impedance plot, we have a skewed semicircle which is followed by an incomplete arc, and these plots are fitted into the [R(RQ)(RQ)] equivalent circuit

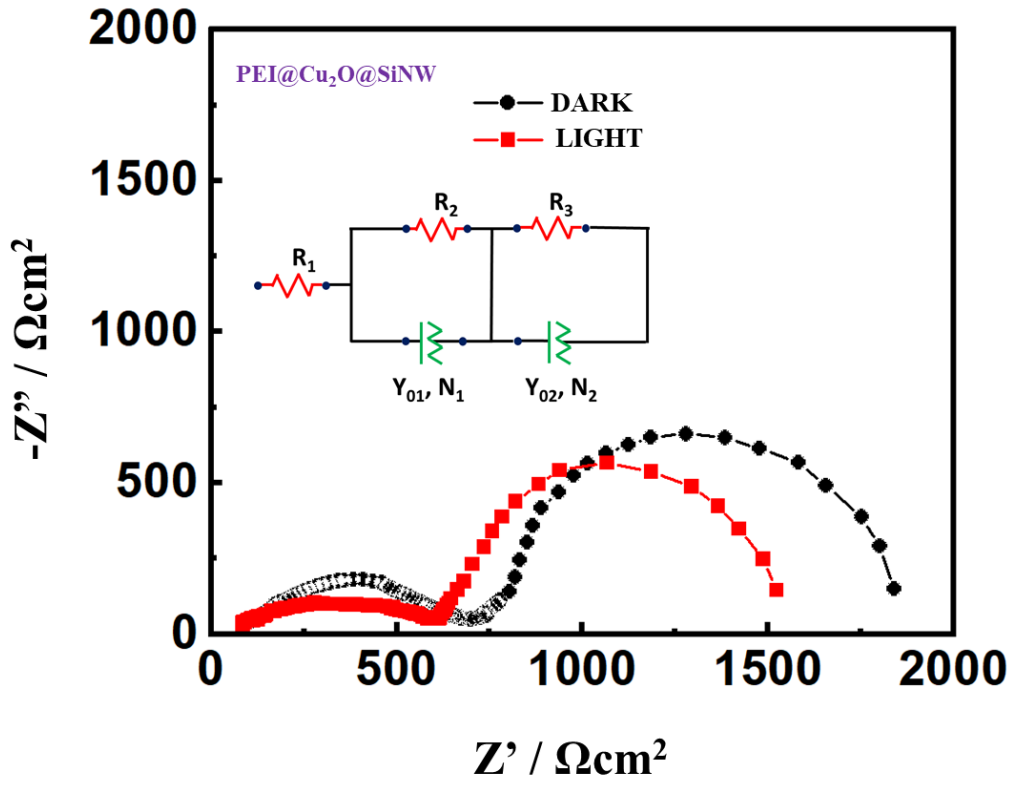

Fig 3.3.2: Nyquist plots of solar cell with photoanode /Br^-/Br_2-C fabric under light (0.5 sun) and dark conditions.

Table 14: Fitted Nyquist parameters of the solar cells under light (0.5 sun) and dark conditions.

Parameters	PEI@Cu_2O@SiNW/ Br^-/Br_2-C fabric light	PEI@Cu_2O@SiNW/ Br^-/Br_2-C fabric dark
R_s (Ω cm^2)	68.42	70.18
R_{ct} (Ω cm^2)	527.89	632.75
R_{rec}(Ω cm^2)	928.24	1141.15

From the above figure, it is clear that when the cell is in the dark, the recombination resistance is 1.036 KΩ, but as soon as the light is illuminated, the recombination resistance decreases and becomes 0.86 KΩ but here the hole transport due to PEI@Cu_2O@SiNW dominates here and helps in efficient charge transport at electrolyte/electrode interface.

3.3.3 Energy Profile Diagram

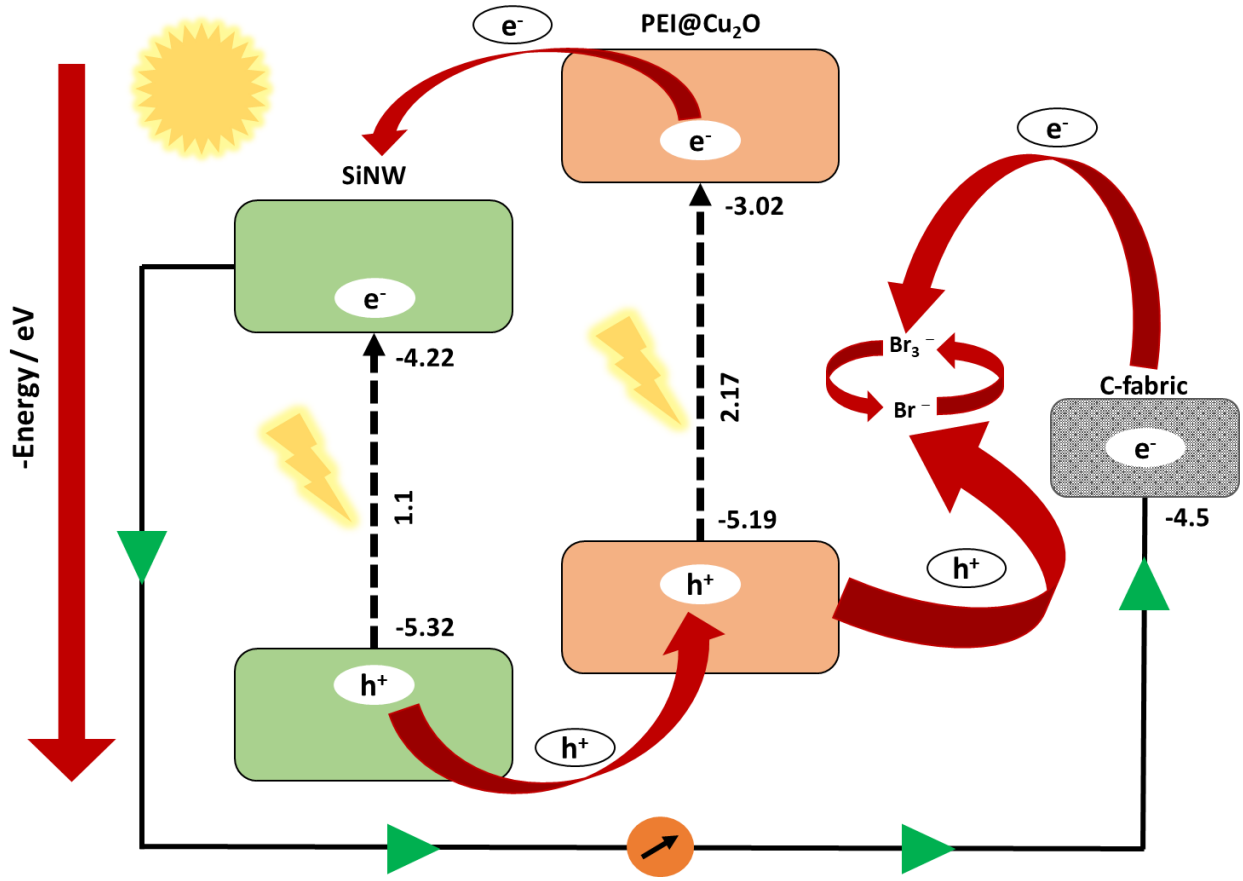

Figure 3.3.3: Energy level diagram of the PEI@Cu_2O@SiNW-Br-/Br2-C fabric solar cell showing all possible modes of electron transfer under 1 sun illumination

The above energy band diagram shows all possible routes for electron transfer in the fabricated solar cell. The band positions, i.e., VBs and CBs are determined using cyclic voltammetry. Under the illumination of light electronic excitation takes place in SiNW, and since the VB and CB of PEI@Cu_2O@SiNW lies above the corresponding bands of SiNW, so electron transfer takes place from the CB of PEI@Cu_2O@SiNW to SiNW, which causes the reduction of redox electrolyte from

Br_3^- to Br^-. The holes generated in the VB of SiNW are transferred to VB of PEI@Cu_2O@SiNW, which act as efficient hole transport, and the transferred hole helps in oxidizing the redox electrode from Br^- to Br_3^-.

4. Conclusion:

For a material to act as efficient hole transport, its HOMO level should lie above the HOMO of SiNW. Since the HOMO level of Cu_2O (-5.5 eV) lies below the HOMO of SiNW (-5.3 eV) so it cannot act as a hole transporter. We decorated Cu_2O with PEI polymer, which decreases the work function of the material without changing its bandgap (2.17 eV). When the Cu_2O microcrystals are decorated with PEI, its HOMO level (-5.19 eV) get aligned above HOMO of SiNW and hence PEI@Cu_2O act as hole transporting material over SiNW. It increases recombination resistance as well as the efficiency of the cell.

REFERENCES

1. J. Conti., *International Energy Outlook*, 2011; U.S. Energy Administration: Washington, DC, 2011.

2. O. Chapin; C. Fuller; G. Pearson *J. Appl. Phys.* 1954, **25**, 676.

3. M. Green; K. Emery; Y. Hishikawa; W. Warta; E. Dunlop *Prog. Photovoltaics Res. Appl.* 2014, **22**, 1.

4. A. Yella; H. Lee; H. Tsao; C. Yi; A. Chandiran; Nazeeruddin, M.; Diau, E.; Yeh, C.; Zakeeruddin, S.; Gratzel, M. *Science* 2011, **334**, 629

5. S. Mathew; A. Yella; P. Gao; R. Humphry-Baker; B. Curchod; N. Ashari-Astani; I. Tavernelli; U. Rothlisberger; M. Nazeeruddin; M. Gratzel, *Nat. Chem.* 2014, **6**, 242.

6. T. Sugaya; O. Numakami; R. Oshima; S. Furue; H. Komaki; T. Amano; K. Matsubara; Y. Okano; S. Niki *Energy Environ. Sci.* 2012, **5**, 6233.

7. Service, R. F. *Science* 2014, **344**, 458.

8. R.S. Wagner., *Applied Physics Letters*, **Vol.4, No.5**, 89-90, 1964.

9. Thomas Mikolajick; Andre Heinzig; Jens Trommer; et al. (2013). *Physica Status Solidi RRL*. **7** (10): 793–799.

10. Z. Huang; H. Fang; J. Zhu (2007). *Advanced Materials*. **19** (5): 744–748.

11. M. Shao; D. Duo Ma; Lee, ST (2010). *European Journal of Inorganic Chemistry*. 2010 **(27)**: 4264–4278.

12. Zhipeng Huang; Nadine Geyer; Peter Werner; Johannes de Boor; Gösele, *Advanced Materials*. **23** (2): 285–308.

13. J. F. Gibbons; G. W. Cogan; C. M. Gronet; N. S. Lewis, *Appl. Phys. Lett.* 1984, **45**, 1095– 1097.

14. A. Bansal; N. S. Lewis, *J. Phys. Chem. B* 1998, **102**, 4058– 4060.

15. K. Peng; X. Wang; S.-T. Lee, *Appl. Phys. Lett.* 2008, **92** (16), 163103.

16. E. A. Dalchiele; F. Martín; D. Leinen; R. E. Marotti; & J. R. Ramos-Barrado, (2009). *Journal of The Electrochemical Society*, **156(5),** K77.

17. K. Peng; X. Wang; X. Wu; S. Lee, *Nano. Lett.* 2009, **9**, 3704– 3709.

18. J. Buch; B. Hammond; *Int. J. Mol. Sci.* 2020, **21**, 8020.

19. M. T. Kibria; A. Ahammed; S. M. Sony; F. Hossain; S. U. Islam, *Proceedings of 5th International Conference on Environmental Aspects of Bangladesh [ICEAB 2014]*.

20. M. A. Green, K. Emery, Y. Hishikawa, W. Warta; E. D. Dunlop, *Prog. Photovolt: Res. Appl.*, 2012, **20**, 12–20.

21. W. H. Bloss; F. Pfisterer; M. Schubert and T. Walter, *Prog. Photovolt: Res. Appl.*, 1995, **3**, 3−24

22. M. A. Green, *Physica E*, 2002, **14**, 65 – 70.

23. J. Yan; B. R. Saunders, *RSC Adv.*, 2014, **4**, 43286

24. W. Shockley; H. J. Queisser, *Journal of Applied Physics* **32**, 510 (1961)

25. M. Florides, *Silicon Nanowires and their Applications*, 2010.

26. T. Mikolajick; A. Heinzig; J. Trommer, *Physica Status Solidi RRL*, 2013, **7** (10), 793–799.

27. Z. Huang; H. Fang; J. Zhu, *Advanced Materials*, 2007, **19** (5): 744–748.

28. Z. Huang; N. Geyer; P. Werner; J. Boor; U. Gösele, *Advanced Materials*, 2011, **23** (2), 285–308.

29. M. Shao; D. Duo Ma; ST. Lee, *European Journal of Inorganic Chemistry*, 2010, **27**, 4264–4278.

30. L. Tsakalakos; J. Balch; J. Fronheiser; B. A. Korevaar, *Appl. Phys. Lett*., 2007, **91**, 233117.

31. P. V. Kamat, K. Tvrdy, D. R. Baker and J. G. Radich, *Chem. Rev*., 2010, **110**, 6664–6688.

32. X. Shen; B. Sun; F. Yan; J. Zhao; F. Zhang; S. Wang; X. Zhu; S. Lee, *ACS Nano* 2010, **4**, 5869– 5876.

33. X. Wang; K.-Q Peng; X.-J. Pan; X. Chen; Y. Yang; L. Li; X.-M. Meng; W.-J. Zhang; S.-T. Lee, *Angew. Chem., Int. Ed.* 2011, **50**, 9861– 9865.

34. R. Jiat; Z. Feng; K. Tao; B. Dou; Y. Sun; & Z. Jin, 2016 IEEE 43rd Photovoltaic Specialists Conference (PVSC). DOI:10.1109/pvsc.2016.7750000

35. Y. Rui, T. Zhang, D. Zhu, Y. Feng, A. N. Cartwright, M. T. Swihart, Y. Yang, T. Zhang, C. Huang, H. Wang, and D. Gu, *The Journal of Physical Chemistry C.*, 2019, DOI: 10.1021/acs.jpcc.8b10542

36. A. Kolay; D. Maity; P. Ghosal; M. Deepa, *J. Phys. Chem. C* 2019, **123**, 8614– 8622.

37. A. Kolay; D. Maity; P. Ghosal & M. Deepa (2019). *ACS Applied Materials & Interfaces.* DOI:10.1021/acsami.9b17573

38. M. Seo et al., *IEEE J. Photovolt.*, **vol. 10**, no. 2, pp. 475– 479, Mar. 2020.

39. V. Smil, *General Energetics: Energy in the Biosphere and Civilization*; John Wiley: New York, 1991; p 240.

40. M. L. Rosenbluth; C. M. Lieber; N. S. Lewis, *Applied Physics Letters*, 1984, **45**, 423.

41. C. M. Lieber; C. M. Gronet; N. S. Lewis, *Nature*, **307**, 533–534(1984).

42. M. L. Rosenbluth; N. S. Lewis *J. Am. Chem. Soc.*, 108, **16**, 1986.

43. J. R. Maiolo III; B. M. Kayes; M. A. Filler; M. C. Putnam; M. D. Kelzenberg; H. A. Atwater; N. S. Lewis, *J. Am. Chem. Soc*. 2007, **129**, 12346-12347.

44. J. R. Maiolo III, H. A. Atwater; N. S. Lewis, *J. Phys. Chem. C*, 112 (15), 2008, **6195**.

45. C. M. Gronet; N. S. Lewis; G. Cogan; J. Gibbons, *Proc. Natl. Acad. Sci*. USA **80** (1983).

46. A. S. Togonal; L. He; P. R. Cabarrocas; Rusli, *Langmuir* 2014, **30**, 10290−10298.

47. H. Y. Zhao; Y. F. Wang; J. H. Zeng, *Crystal Growth & Design*, 8, **10**, 2008.

48. Y. Zhou; C. F. Hernandez; J. Shim; J. Meyer; A. J. Giordano; H. Li; P. Winget; T. Papadopoulos; H. Cheun; J. Kim; M. Fenoll; A. Dindar; W. Haske; E. Najafabadi; T. M. Khan; H. Sojoudi; S. Barlow; S. Graham; J. L. Brédas; S. R. Marder; A. Kahn; B. Kippelen, *Science* Vol **336** 20 April 2012.

Pictures bibliography

Fig 1.1.2: https://en.wikipedia.org/wiki/Silicon#/media/File:Covalent_bonding_in_silicon.svg

Fig 1.1.4: a) https://en.wikipedia.org/wiki/Air_mass_(solar_energy)#/media/File:Solar_Spectrum.png

b) https://www.enlitechnology.com/show/air-mass-am1-5g-am1-5d-306249.htm

Fig 1.2: a) https://www.researchgate.net/publication/285042969_Electric_Energy_Management_ and_ Engineering_in_Solar_Cell_System/figures? lo=1

b) https://www.alternative-energy-tutorials.com/photovoltaics/solar-cell-i-v-characteristic.html

Fig 1.3.1: https://www.pveducation.org/pvcdrom/solar-cell-operation/open-circuit-voltage

Fig 1.7: https://en.wikipedia.org/wiki/Shockley%E2%80%93Queisser_limit#/media/File:Shockley QueisserFullCurve.svg

Fig 1.7.3: https://en.wikipedia.org/wiki/Shockley%E2%80%93Queisser_limit#/media/File:Shockley QueisserBreakdown2.svg